

# Machine Learning the Dimension of a Fano Variety

Tom Coates<sup>a,1</sup>, Alexander M. Kasprzyk<sup>b,1</sup>, and Sara Veneziale<sup>a,1,2</sup>

<sup>a</sup>Department of Mathematics, Imperial College London, 180 Queen's Gate, London SW7 2AZ, United Kingdom; <sup>b</sup>School of Mathematical Sciences, University of Nottingham, Nottingham NG7 2RD, United Kingdom

This manuscript was compiled on December 16, 2022

1 **Fano varieties are basic building blocks in geometry – they are**  
2 ‘atomic pieces’ of mathematical shapes. Recent progress in the clas-  
3 sification of Fano varieties involves analysing the quantum period of  
4 a Fano variety  $X$ . This is a power series determined by  $X$  whose  
5 coefficients, which are a sequence of integers, give a numerical sig-  
6 nature for  $X$ . We apply machine learning to the question: does the  
7 quantum period of a Fano variety  $X$  know the dimension of  $X$ ? Note  
8 that there is as yet no theoretical understanding of this. We show  
9 that Support Vector Machine methods can determine the dimension  
10 of  $X$  from its quantum period with 87.7% accuracy, and that a Deep  
11 Neural Network can determine the dimension with 89.0% accuracy.  
12 Inspired by this, we establish rigorous asymptotics for the quantum  
13 periods of Fano toric varieties with low Picard rank. These asymp-  
14 totics determine the dimension of  $X$  from its quantum period. This  
15 demonstrates that machine learning can pick out structure from com-  
16 plex mathematical data in situations where we lack a theoretical un-  
17 derstanding. It also gives positive evidence for the assertion (which  
18 is proven for smooth varieties in low dimensions but unknown in  
19 general) that the quantum period of a Fano variety determines that  
20 variety.

Fano varieties | quantum periods | mirror symmetry | machine learning

1 **A**lgebraic geometry describes shapes as the solution sets  
2 of systems of polynomial equations, and manipulates or  
3 analyses a shape  $X$  by manipulating or analysing the equations  
4 that define  $X$ . This interplay between algebra and geometry  
5 has applications across mathematics and science; see e.g. (1–4).  
6 Shapes defined by polynomial equations are called *algebraic*  
7 *varieties*. Fano varieties are a particularly important class of  
8 algebraic varieties. They are, in a precise sense, atomic pieces  
9 of mathematical shapes (5, 6), and their classification is a  
10 long-standing open problem (7–13).

11 A new approach to the classification of Fano varieties centres  
12 around a set of ideas from string theory called Mirror  
13 Symmetry (14–17). From this perspective, the key invariant  
14 of a Fano variety is its *regularized quantum period* (18)

$$\widehat{G}_X(t) = \sum_{d=0}^{\infty} c_d t^d \quad [1]$$

16 This is a power series with coefficients  $c_0 = 1$ ,  $c_1 = 0$ , and  
17  $c_d = r_d d!$ , where  $r_d$  is a certain Gromov–Witten invariant  
18 of  $X$ . Intuitively speaking,  $r_d$  is the number of rational curves  
19 in  $X$  of degree  $d \geq 2$  that pass through a fixed generic point  
20 and have a certain constraint on their complex structure. In  
21 general  $r_d$  can be a rational number, because curves with a  
22 symmetry group of order  $k$  are counted with weight  $1/k$ , but  
23 in all known cases the coefficients  $c_d$  in Eq. (1) are integers.

24 In this paper we will treat the regularized quantum period  
25 as a numerical signature for the Fano variety  $X$ , given by

26 the sequence of integers  $(c_0, c_1, \dots)$ . *A priori* this looks like  
27 an infinite amount of data, but in fact there is a differential  
28 operator  $L$  such that  $L\widehat{G}_X \equiv 0$ ; see e.g. (18, Theorem 4.3).  
29 This gives a recurrence relation that determines all of the coeffi-  
30 cients  $c_d$  from the first few terms, so the quantum period  $\widehat{G}_X$   
31 contains only a finite amount of information. Encoding a  
32 Fano variety  $X$  by a vector in  $\mathbb{Z}^{m+1}$  given by finitely many  
33 coefficients  $(c_0, c_1, \dots, c_m)$  of the regularized quantum period  
34 allows us to apply machine learning methods to questions  
35 about Fano varieties.

36 It is unknown whether the regularized quantum period of  
37 a Fano variety  $X$  uniquely identifies  $X$ . This is true (and  
38 proven) for smooth Fano varieties in low dimensions, but is  
39 unknown in dimensions four and higher. As a first step, in this  
40 paper we ask whether the regularized quantum period of a  
41 Fano variety  $X$  knows the dimension of  $X$ . There is currently  
42 no viable theoretical approach to this question. Instead we use  
43 machine learning methods applied to a large dataset to argue  
44 that the answer is probably yes, and then establish new (and  
45 rigorous) asymptotic results that relate the quantum periods  
46 of toric Fano varieties with low Picard rank to their dimension.  
47 This work is also proof-of-concept for a larger program, showing  
48 that machine learning can uncover previously unknown  
49 structure in complex mathematical datasets. Thus the Data  
50 Revolution, which has had such impact across the rest of  
51 science, also brings important new insights to pure mathemat-  
52 ics (19). This is particularly true for large-scale classification  
53 questions, of which there are many: see e.g. (20–24), where  
54 these methods can potentially reveal both the classification  
55 itself and structural relationships within it.

## Significance Statement

Fano varieties are basic building blocks in geometry – they are ‘atomic pieces’ of mathematical shapes. Recent progress in the classification of Fano varieties involves analysing an invariant called the quantum period. This is a sequence of integers which gives a numerical fingerprint for a Fano variety. It is conjectured that a Fano variety is uniquely determined by its quantum period. If this is true, one should be able to recover geometric properties of a Fano variety directly from its quantum period. We use machine learning methods to determine the dimensions of Fano varieties from their quantum periods. This shows that machine learning can pick out structure from complex pure-mathematical data, and gives evidence for the conjecture.

The authors declare no competing interest.

<sup>1</sup>All authors contributed equally to this work.

<sup>2</sup>To whom correspondence should be addressed. E-mail: s.veneziale21@imperial.ac.uk

**The Fano varieties that we consider.** The fundamental example of a Fano variety is projective space  $\mathbb{P}^{N-1}$ . This is a quotient of  $\mathbb{C}^N \setminus \{0\}$  by the group  $\mathbb{C}^\times$ , where the action of  $\lambda \in \mathbb{C}^\times$  identifies the points  $(x_1, x_2, \dots, x_N)$  and  $(\lambda x_1, \lambda x_2, \dots, \lambda x_N)$ . The resulting algebraic variety has dimension  $N - 1$ . We will consider generalisations of projective spaces called *weighted projective spaces* and *toric varieties of Picard rank two*. A detailed introduction to these spaces is given in the Supplementary Material.

To define a weighted projective space, choose positive integers  $a_1, a_2, \dots, a_N$  such that any subset of size  $N - 1$  has no common factor, and consider

$$\mathbb{P}(a_1, a_2, \dots, a_N) = (\mathbb{C}^N \setminus \{0\}) / \mathbb{C}^\times$$

where the action of  $\lambda \in \mathbb{C}^\times$  identifies the points

$$(x_1, x_2, \dots, x_N) \quad \text{and} \quad (\lambda^{a_1} x_1, \lambda^{a_2} x_2, \dots, \lambda^{a_N} x_N)$$

in  $\mathbb{C}^N \setminus \{0\}$ . The quotient  $\mathbb{P}(a_1, a_2, \dots, a_N)$  is an algebraic variety of dimension  $N - 1$ . A general point of  $\mathbb{P}(a_1, a_2, \dots, a_N)$  is smooth, but there can be singular points. Indeed, a weighted projective space  $\mathbb{P}(a_1, a_2, \dots, a_N)$  is smooth if and only if  $a_i = 1$  for all  $i$ , that is, if and only if it is a projective space.

To define a toric variety of Picard rank two, choose a matrix

$$\begin{pmatrix} a_1 & a_2 & \cdots & a_N \\ b_1 & b_2 & \cdots & b_N \end{pmatrix} \quad [2]$$

with non-negative integer entries and no zero columns. This defines an action of  $\mathbb{C}^\times \times \mathbb{C}^\times$  on  $\mathbb{C}^N$ , where  $(\lambda, \mu) \in \mathbb{C}^\times \times \mathbb{C}^\times$  identifies the points

$$(x_1, x_2, \dots, x_N) \quad \text{and} \quad (\lambda^{a_1} \mu^{b_1} x_1, \lambda^{a_2} \mu^{b_2} x_2, \dots, \lambda^{a_N} \mu^{b_N} x_N)$$

in  $\mathbb{C}^N$ . Set  $a = a_1 + a_2 + \dots + a_N$  and  $b = b_1 + b_2 + \dots + b_N$ , and suppose that  $(a, b)$  is not a scalar multiple of  $(a_i, b_i)$  for any  $i$ . This determines linear subspaces

$$\begin{aligned} S_+ &= \{(x_1, x_2, \dots, x_N) \mid x_i = 0 \text{ if } b_i/a_i < b/a\} \\ S_- &= \{(x_1, x_2, \dots, x_N) \mid x_i = 0 \text{ if } b_i/a_i > b/a\} \end{aligned}$$

of  $\mathbb{C}^N$ , and we consider the quotient

$$X = (\mathbb{C}^N \setminus S) / (\mathbb{C}^\times \times \mathbb{C}^\times) \quad [3]$$

where  $S = S_+ \cup S_-$ . The quotient  $X$  is an algebraic variety of dimension  $N - 2$  and second Betti number  $b_2(X) \leq 2$ . If, as we assume henceforth, the subspaces  $S_+$  and  $S_-$  both have dimension two or more then  $b_2(X) = 2$ , and thus  $X$  has Picard rank two. In general  $X$  will have singular points, the precise form of which is determined by the weights in Eq. (2).

There are closed formulas for the regularized quantum period of weighted projective spaces and toric varieties (25). We have

$$\widehat{G}_\mathbb{P}(t) = \sum_{k=0}^{\infty} \frac{(ak)!}{(a_1 k)! (a_2 k)! \cdots (a_N k)!} t^{ak} \quad [4]$$

where  $\mathbb{P} = \mathbb{P}(a_1, \dots, a_N)$  and  $a = a_1 + a_2 + \dots + a_N$ , and

$$\widehat{G}_X(t) = \sum_{(k,l) \in \mathbb{Z}^2 \cap C} \frac{(ak + bl)!}{(a_1 k + b_1 l)! \cdots (a_N k + b_N l)!} t^{ak + bl} \quad [5]$$

where the weights for  $X$  are as in Eq. (2), and  $C$  is the cone in  $\mathbb{R}^2$  defined by the equations  $a_i x + b_i y \geq 0$ ,  $i \in \{1, 2, \dots, N\}$ .

In our data analysis, we restricted attention to weighted projective spaces and toric varieties with *terminal quotient singularities*. These singularities, introduced by Reid, play a fundamental role in birational geometry (26, 27). Terminal quotient singularities are very mild; indeed, in dimensions one and two, an algebraic variety has terminal quotient singularities if and only if it is smooth.

**Data generation: weighted projective spaces.** All singularities of weighted projective spaces are quotient singularities. The following result characterises weighted projective spaces with terminal singularities; this is (28, Proposition 2.3).

**Proposition 1.** Let  $X = \mathbb{P}(a_1, a_2, \dots, a_N)$  be a weighted projective space of dimension at least three. Then  $X$  has at worst terminal singularities if and only if

$$\sum_{i=1}^N \{ka_i/a\} \in \{2, \dots, N-2\} \quad [106]$$

for each  $k \in \{2, \dots, a-2\}$ . Here  $a = a_1 + a_2 + \dots + a_N$  and  $\{q\}$  denotes the fractional part  $q - \lfloor q \rfloor$  of  $q \in \mathbb{Q}$ .

A simpler necessary condition is given by (29, Theorem 3.5):

**Proposition 2.** Let  $X = \mathbb{P}(a_1, a_2, \dots, a_N)$  be a weighted projective space of dimension at least two, with weights ordered  $a_1 \leq a_2 \leq \dots \leq a_N$ . If  $X$  has at worst terminal singularities then  $a_i/a < 1/(N-i+2)$  for each  $i \in \{3, \dots, N\}$ .

Weighted projective spaces with terminal singularities have been classified in dimensions up to four (28, 30). Classifications in higher dimensions are hindered by the lack of an effective upper bound on  $a$ .

We randomly generated 150 000 distinct weighted projective spaces with at worst terminal singularities, and with dimension up to 10, as follows. We generated random sequences of weights  $a_1 \leq a_2 \leq \dots \leq a_N$  with  $a_N \leq 10N$  and discarded them if they failed to satisfy any one of the following:

1. for each  $i \in \{1, \dots, N\}$ ,  $\gcd\{a_1, \dots, \widehat{a}_i, \dots, a_N\} = 1$ , where  $\widehat{a}_i$  indicates that  $a_i$  is omitted;
2.  $a_i/a < 1/(N-i+2)$  for each  $i \in \{3, \dots, N\}$ ;
3.  $\sum_{i=1}^N \{ka_i/a\} \in \{2, \dots, N-2\}$  for each  $k \in \{2, \dots, a-2\}$ .

Condition 1 here was part of our definition of weighted projective spaces above; it ensures that the set of singular points in  $\mathbb{P}(a_1, a_2, \dots, a_N)$  has dimension at most  $N-2$ , and also that weighted projective spaces are isomorphic as algebraic varieties if and only if they have the same weights. Condition 2 is from Proposition 2; it efficiently rules out many non-terminal examples. Condition 3 is the necessary and sufficient condition for terminality from Proposition 1. We then deduplicated the sequences. The resulting sample sizes are summarised in Table 1. The sample data (31), along with the code for the Magma computer algebra system (32) that was used to generate it, is available from Zenodo (33) under a Creative Commons CC0 license. The data was collected using Magma V2.25-4.

Weighted projective spaces			Rank-two toric varieties		
Dimension	Sample size	Percentage	Dimension	Sample size	Percentage
1	1	0.001	2	2	0.001
2	1	0.001	3	17	0.009
3	7	0.005	4	758	0.379
5	23 584	15.723	6	6 050	3.025
6	23 640	15.760	7	19 690	9.845
7	23 700	15.800	8	35 395	17.698
8	23 469	15.646	9	42 866	21.433
9	23 225	15.483	10	47 206	23.603
10	23 437	15.625		48 016	24.008
Total	150 000		Total	200 000	

**Table 1.** The number and percentage of terminal weighted projective spaces and toric varieties of Picard rank two appearing in the sample data.

140 **Data generation: toric varieties of Picard rank 2.** Deduplicating 141 randomly-generated toric varieties of Picard rank two is 142 harder than deduplicating randomly generated weighted 143 projective spaces, because different weight matrices in Eq. (2) 144 can give rise to the same toric variety. Toric varieties are 145 uniquely determined, up to isomorphism, by a combinatorial 146 object called a *fan* (34). A fan is a collection of cones, and 147 one can determine the singularities of a toric variety  $X$  from 148 the geometry of the cones in the corresponding fan.

149 We randomly generated 200 000 distinct toric varieties of 150 Picard rank two with at worst terminal singularities, and 151 with dimension up to 10, as follows. We randomly generated 152 weight matrices, as in Eq. (2), such that  $0 \leq a_i, b_j \leq 5$ . We 153 then discarded the weight matrix if any column was zero, and 154 otherwise formed the corresponding fan  $F$ . We discarded the 155 weight matrix unless:

- 156 1. each cone in  $F$  was simplicial (i.e. has number of rays 157 equal to its dimension);
- 158 2.  $F$  had  $N$  rays;
- 159 3. the convex hull of the primitive generators of the rays 160 of  $F$  contained no lattice points other than the rays and 161 the origin.

162 Condition 1 here guarantees that the corresponding toric variety 163  $X$  has  $\mathbb{Q}$ -factorial quotient singularities. Conditions 1 164 and 2 together guarantee that  $X$  has Picard rank two, and are 165 equivalent to the conditions on the weight matrix in Eq. (2) 166 given in our definition. Condition 3 holds if and only if  $X$  has 167 terminal singularities. We then deduplicated the weight matrices 168 according to the isomorphism type of  $F$ , by putting  $F$  in 169 normal form (35, 36). The sample data (37) and the Magma 170 code used to generate it is available from Zenodo under a CC0 171 license. See Table 1 for a summary of the dataset.

172 **Data analysis: weighted projective spaces.** We began by 173 computing an initial segment  $(c_0, c_1, \dots, c_m)$  of the regularized 174 quantum period for all the examples in the sample of 150 000 175 terminal weighted projective spaces, with  $m \approx 100 000$ . The 176 non-zero coefficients  $c_d$  appeared to grow exponentially with  $d$ , 177 and so we considered  $\{\log c_d\}_{d \in S}$  where  $S = \{d \in \mathbb{Z}_{\geq 0} \mid c_d \neq 178 0\}$ . To reduce dimension we fitted a linear model to the 179 set  $\{(d, \log c_d) \mid d \in S\}$  and used the slope and intercept of

180 this model as features; see Figure 1 for a typical example. Plotting 181 the slope against the  $y$ -intercept and colouring datapoints 182 according to the dimension we obtain Figure 2: note the clear 183 separation by dimension. A Support Vector Machine (SVM) 184 trained on 10% of the slope and  $y$ -intercept data predicted the 185 dimension of the weighted projective space with an accuracy 186 of 99.99%. Full details are given in the Supporting Material.

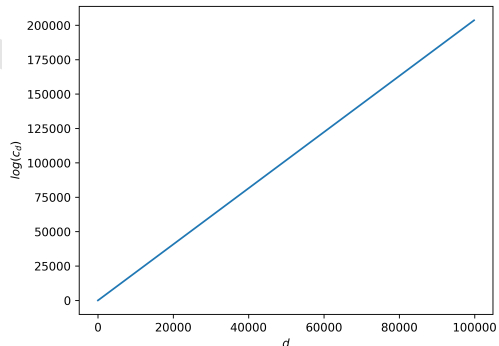


**Fig. 1.** The logarithm of the non-zero period coefficients  $c_d$  for a typical example: the weighted projective space  $\mathbb{P}(5, 5, 11, 23, 28, 29, 33, 44, 66, 76)$ .

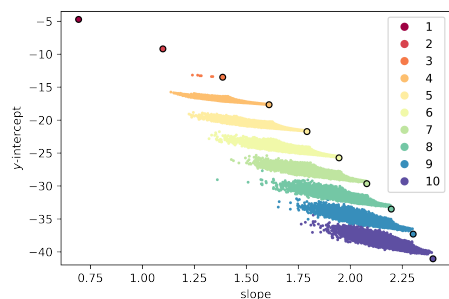


**Fig. 2.** The slopes and  $y$ -intercepts from the linear model applied to weighted projective spaces with terminal singularities. The colour records the dimension of the weighted projective space. The circled points indicate projective spaces.

187 **Data analysis: toric varieties of Picard rank 2.** As before, the  
188 non-zero coefficients  $c_d$  appeared to grow exponentially with  $d$ ,  
189 so we fitted a linear model to the set  $\{(d, \log c_d) \mid d \in S\}$   
190 where  $S = \{d \in \mathbb{Z}_{\geq 0} \mid c_d \neq 0\}$ . We used the slope and  
191 intercept of this linear model as features.

192 **Example 3.** In Figure 3 we plot a typical example: the  
193 logarithm of the regularized quantum period sequence for the  
194 nine-dimensional toric variety with weight matrix

$$\begin{pmatrix} 1 & 2 & 5 & 3 & 3 & 3 & 0 & 0 & 0 & 0 \\ 0 & 0 & 0 & 3 & 4 & 4 & 1 & 2 & 2 & 3 & 4 \end{pmatrix}$$

195 along with the linear approximation. We see a periodic deviation  
196 from the linear approximation; the magnitude of this  
197 deviation decreases as  $d$  increases (not shown).

198 To reduce computational costs, we computed  
199 pairs  $(d, \log c_d)$  for  $1000 \leq d \leq 20000$  by sampling every  
200 100th term. We discarded the beginning of the period  
201 sequence because of the noise it introduces to the linear  
202 regression. In cases where the sampled coefficient  $c_d$  is zero,  
203 we considered instead the next non-zero coefficient. The  
204 resulting plot of slope against  $y$ -intercept, with datapoints  
205 coloured according to dimension, is shown in Figure 4.

206 We analysed the standard errors for the slope and  
207  $y$ -intercept of the linear model. The standard errors for the  
208 slope are small compared to the range of slopes, but in many  
209 cases the standard error  $s_{\text{int}}$  for the  $y$ -intercept is relatively  
210 large. As Figure 5 illustrates, discarding data points where the  
211 standard error  $s_{\text{int}}$  for the  $y$ -intercept exceeds some threshold  
212 reduces apparent noise. This suggests that the underlying  
213 structure is being obscured by inaccuracies in the linear regres-  
214 sion caused by oscillatory behaviour in the initial terms of the  
215 quantum period sequence; these inaccuracies are concentrated  
216 in the  $y$ -intercept of the linear model. Note that restricting  
217 attention to those data points where  $s_{\text{int}}$  is small also greatly  
218 decreases the range of  $y$ -intercepts that occur. As Example 4  
219 and Figure 6 suggest, this reflects both transient oscillatory  
220 behaviour and also the presence of a subleading term in the  
221 asymptotics of  $\log c_d$  which is missing from our feature set.  
222 We discuss this further below.

223 **Example 4.** Consider the toric variety with Picard rank two  
224 and weight matrix

$$\begin{pmatrix} 1 & 10 & 5 & 13 & 8 & 12 & 0 \\ 0 & 0 & 3 & 8 & 5 & 14 & 1 \end{pmatrix}$$

225 This is one of the outliers in Figure 4. The toric variety is  
226 five-dimensional, and has slope 1.637 and  $y$ -intercept  $-62.64$ .  
227 The standard errors are  $4.246 \times 10^{-4}$  for the slope and 5.021 for  
228 the  $y$ -intercept. We computed the first 40 000 coefficients  $c_d$   
229 in Eq. (1). As Figure 6 shows, as  $d$  increases the  $y$ -intercept  
230 of the linear model increases to  $-28.96$  and  $s_{\text{int}}$  decreases  
231 to 0.7877. At the same time, the slope of the linear model  
232 remains more or less unchanged, decreasing to 1.635. This  
233 supports the idea that computing (many) more coefficients  $c_d$   
234 would significantly reduce noise in Figure 4. In this example,  
235 even 40 000 coefficients may not be enough.

236 Computing many more coefficients  $c_d$  across the whole  
237 dataset would require impractical amounts of computation  
238 time. In the example above, which is typical in this regard,  
239 increasing the number of coefficients computed from 20 000

240 to 40 000 increased the computation time by a factor of more  
241 than 10. Instead we restrict to those toric varieties of Pi-  
242 card rank two such that the  $y$ -intercept standard error  $s_{\text{int}}$   
243 is less than 0.3; this retains 67 443 of the 200 000 datapoints.  
244 We used 70% of the slope and  $y$ -intercept data in the re-  
245 stricted dataset for model training, and the rest for validation.  
246 An SVM model predicted the dimension of the toric variety  
247 with an accuracy of 87.69%; a Random Forest Classifier (RFC)  
248 model predicted the dimension with an accuracy of 88.61%;  
249 and a Multilayer Perceptron (MLP) with three hidden layers  
250

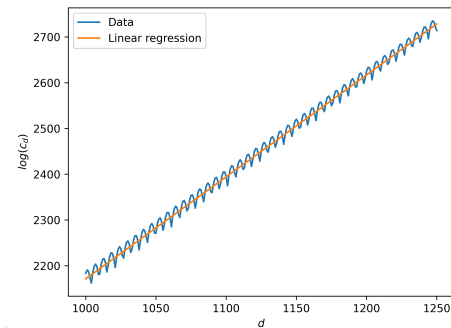


**Fig. 3.** The logarithm of the non-zero period coefficients  $c_d$  for Example 3, together with its linear approximation.

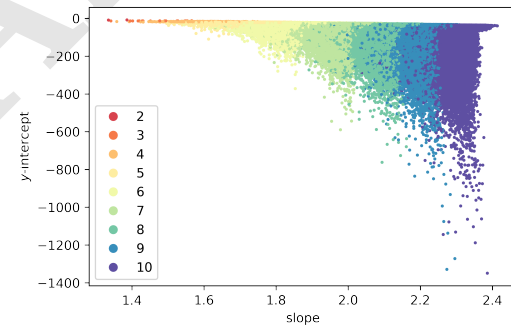


**Fig. 4.** The slopes and  $y$ -intercepts from the linear model applied to toric varieties of Picard rank two with terminal singularities. The colour records the dimension of the toric variety.

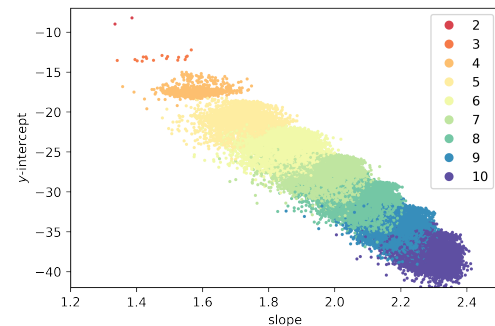


**Fig. 5.** The slopes and  $y$ -intercepts from the linear model as in Figure 4, plotting only data points for which the standard error  $s_{\text{int}}$  for the  $y$ -intercept satisfies  $s_{\text{int}} < 0.3$ . The colour records the dimension of the toric variety.

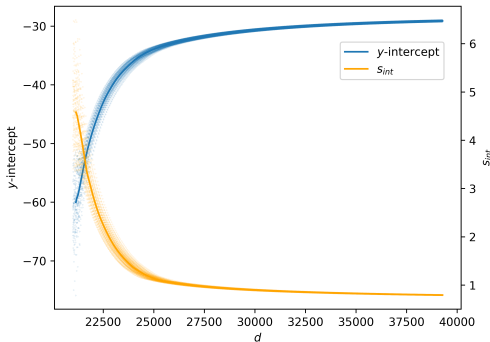


**Fig. 6.** The  $y$ -intercept and standard error  $s_{\text{int}}$  for the rank-two toric variety from Example 4, computed from pairs  $(k, \log c_k)$  such that  $d - 20000 \leq k \leq d$  by sampling every 100th term, together with a LOWESS-smoothed trend line.

predicted the dimension with an accuracy of 89.03%. Full details can be found in the Supplementary Material.

**Rigorous asymptotics for the regularized quantum period.** In the Supplementary Material we establish asymptotic results for the regularized quantum period of toric varieties with low Picard rank, as follows. These results apply to any weighted projective space or toric variety of Picard rank two: they do not require a terminality hypothesis. Note, in each case, the presence of a subleading logarithmic term in the asymptotics for  $\log c_d$ . This term was omitted in the naïve analysis above.

**Theorem 5.** Let  $X$  denote the weighted projective space  $\mathbb{P}(a_1, \dots, a_N)$ , so that the dimension of  $X$  is  $N - 1$ . Let  $c_d$  denote the coefficient of  $t^d$  in the regularized quantum period  $\widehat{G}_X(t)$  given in Eq. (4). Let  $a = a_1 + \dots + a_N$  and  $p_i = a_i/a$ . Then  $c_d = 0$  unless  $d$  is divisible by  $a$ , and non-zero coefficients  $c_d$  satisfy

$$\log c_d \sim Ad - \frac{\dim X}{2} \log d + B$$

as  $d \rightarrow \infty$ , where

$$A = - \sum_{i=1}^N p_i \log p_i$$

$$B = - \frac{\dim X}{2} \log(2\pi) - \frac{1}{2} \sum_{i=1}^N \log p_i$$

Note, although it plays no role in what follows, that  $A$  is the Shannon entropy of the discrete random variable  $Z$  with distribution  $(p_1, p_2, \dots, p_N)$ , and that  $B$  is a constant plus half the total self-information of  $Z$ .

**Theorem 6.** Let  $X$  denote the toric variety of Picard rank two with weight matrix

$$\begin{pmatrix} a_1 & a_2 & a_3 & \cdots & a_N \\ b_1 & b_2 & b_3 & \cdots & b_N \end{pmatrix}$$

so that the dimension of  $X$  is  $N - 2$ . Let  $a = a_1 + \dots + a_N$ ,  $b = b_1 + \dots + b_N$ , and  $\ell = \gcd\{a, b\}$ . Let  $[\mu : \nu] \in \mathbb{P}^1$  be the unique root of the homogeneous polynomial

$$\prod_{i=1}^N (a_i \mu + b_i \nu)^{a_i b} - \prod_{i=1}^N (a_i \mu + b_i \nu)^{b_i a}$$

such that  $a_i \mu + b_i \nu \geq 0$  for all  $i \in \{1, 2, \dots, N\}$ , and set

$$p_i = \frac{\mu a_i + \nu b_i}{\mu a + \nu b}$$

Let  $c_d$  denote the coefficient of  $t^d$  in the regularized quantum period  $\widehat{G}_X(t)$  given in Eq. (5). Then non-zero coefficients  $c_d$  satisfy

$$\log c_d \sim Ad - \frac{\dim X}{2} \log d + B$$

as  $d \rightarrow \infty$ , where

$$A = - \sum_{i=1}^N p_i \log p_i$$

$$B = - \frac{\dim X}{2} \log(2\pi) - \frac{1}{2} \sum_{i=1}^N \log p_i - \frac{1}{2} \log \left( \sum_{i=1}^N \frac{(a_i b - b_i a)^2}{\ell^2 p_i} \right)$$

Theorem 5 is a straightforward application of Stirling's formula. Theorem 6 is more involved, and relies on a Central Limit-type theorem that generalises the De Moivre–Laplace theorem.

**Theoretical analysis.** The asymptotics in Theorems 5 and 6 imply that, for  $X$  a weighted projective space or toric variety of Picard rank two, the quantum period determines the dimension of  $X$ . Let us revisit the clustering analysis from this perspective. Recall the asymptotic expression  $\log c_d \sim Ad - \frac{\dim X}{2} \log d + B$  and the formulae for  $A$  and  $B$  from Theorem 5. Figure 7 shows the values of  $A$  and  $B$  for a sample of weighted projective spaces, colored by dimension. Note the clusters, which overlap.

Consider for example the cluster for weighted projective spaces of dimension five, as in Figure 8. Fix a suitable  $\theta \geq 0$  and consider

$$B + \theta A = - \frac{\dim X}{2} \log(2\pi) - \frac{1}{2} \sum_{i=1}^N \log p_i - \theta \sum_{i=1}^N p_i \log p_i$$

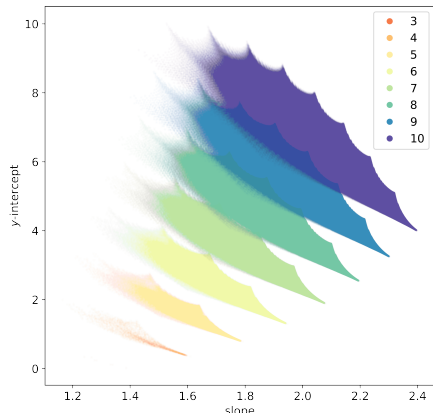


**Fig. 7.** The values of  $A$  and  $B$  for all weighted projective spaces  $\mathbb{P}(a_1, \dots, a_N)$  with terminal singularities and  $a_i \leq 25$  for all  $i$ , coloured by dimension.

with  $\dim X = N - 1 = 5$ . Solving the constrained optimisation problem

$$\min(B + \theta A) \quad \text{subject to} \quad p_1 + \dots + p_6 = 1 \\ p_1, \dots, p_6 \geq 0$$

on the five-simplex gives a linear lower bound for the cluster. This bound does not use terminality: it applies to any weighted projective space of dimension five. The expression  $B + \theta A$  is unbounded above on the five-simplex (because  $B$  is) so we cannot obtain an upper bound this way. Instead, consider

$$\max(B + \theta A) \quad \text{subject to} \quad p_1 + \dots + p_6 = 1 \\ \epsilon \leq p_1 \leq p_2 \leq \dots \leq p_6$$

for an appropriate small positive  $\epsilon$ , which we can take to be  $1/a$  where  $a$  is the maximum sum of the weights. For Figure 8, for example, we can take  $a = 124$ , and in general such an  $a$  exists because there are only finitely many terminal weighted projective spaces. This gives a linear upper bound for the cluster. For example:

**Proposition 7** (which is illustrated in Figure 8). *Let  $X$  be the five-dimensional weighted projective space  $\mathbb{P}(a_1, \dots, a_6)$ , and let  $A, B$  be as in Theorem 5. Then  $B + \frac{5}{2}A \geq \frac{41}{8}$ . If in addition  $a_i \leq 25$  for all  $i$  then  $B + 5A \leq \frac{41}{40}$ .*

The same methods yield linear bounds on each of the clusters in Figure 7. As the Figure shows however, the clusters are not linearly separable.

We see that in Figure 7 broadly speaking the values of  $B$  increase as the dimension of the weighted projective space increases, whereas in Figure 2 the  $y$ -intercepts decrease as the dimension increases. This reflects the fact that we fitted a linear model to  $\log c_d$ , omitting the subleading  $\log d$  term in the asymptotics. The log term does not vary too much over the range of degrees ( $d < 100\,000$ ) that we considered, and has the effect of reducing the observed  $y$ -intercept from  $B$  to approximately  $B - \frac{11}{2} \dim X$ , distorting the clusters slightly and translating them downwards by a dimension-dependent

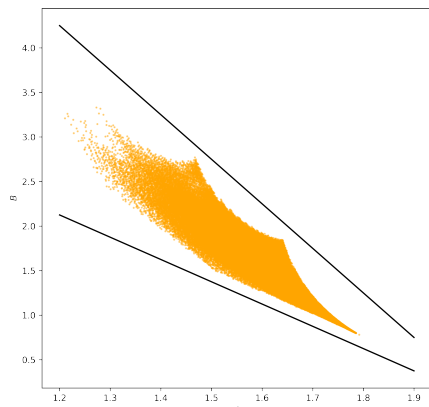


**Fig. 8.** Linear bounds for the cluster given by weighted projective spaces  $\mathbb{P}(a_1, \dots, a_6)$  with terminal singularities and  $a_i \leq 25$  for all  $i$ , given by Prop. 7.

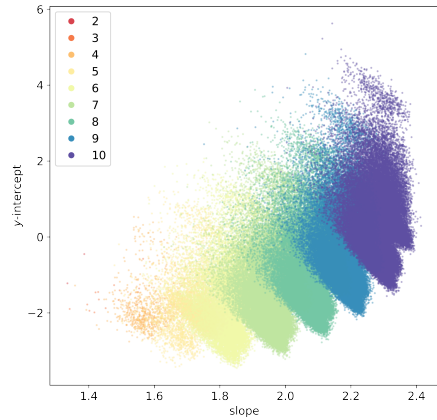


**Fig. 9.** The values of  $A$  and  $B$  for toric varieties of Picard rank two in our dataset, coloured by dimension.

factor. This separates the clusters. We expect that the same mechanism applies in Picard rank two as well: see Figure 9.

**Conclusion.** We developed machine learning models that predict, with high accuracy, the dimension of a Fano variety from its regularized quantum period. These models apply to weighted projective spaces and toric varieties of Picard rank two, with at worst terminal singularities. We then established rigorous asymptotics for the regularized quantum period of these Fano varieties. The form of the asymptotics implies that, in these cases, the regularized quantum period of a Fano variety  $X$  determines the dimension of  $X$ . The asymptotics also give a theoretical underpinning for the success of the machine learning models.

Perversely, because the series involved converge extremely slowly, reading the dimension of a Fano variety directly from the asymptotics of the regularized quantum period is not practical. For the same reason, enhancing the feature set of our machine learning models by including a  $\log d$  term in the linear regression results in less accurate predictions. So although the asymptotics in Theorems 5 and 6 determine the dimension in theory, in practice the most effective way to determine the dimension of an unknown Fano variety from its quantum period is to apply a machine learning model.

This work demonstrates that machine learning can uncover previously unknown structure in complex mathematical data, and is a powerful tool for developing rigorous mathematical results; cf. (19). It also provides evidence for a fundamental conjecture in the Fano classification program (18): that the regularized quantum period of a Fano variety determines that variety.

**ACKNOWLEDGMENTS.** TC is funded by ERC Consolidator Grant 682603 and EPSRC Programme Grant EP/N03189X/1. AK is funded by EPSRC Fellowship EP/N022513/1. SV is funded by the EPSRC Centre for Doctoral Training in Geometry and Number Theory at the Interface, grant number EP/L015234/1. We thank Giuseppe Pitton for conversations and experiments that began this project, and thank John Aston and Louis Christie for insightful conversations and feedback.

- 364 1. van Lint JH, van der Geer G (1988) *Introduction to coding theory and algebraic geometry*,  
 365 DMV Seminar. (Birkhäuser Verlag, Basel) Vol. 12, p. 83.
- 366 2. Niederreiter H, Xing C (2009) *Algebraic geometry in coding theory and cryptography*. (Princeton  
 367 University Press, Princeton, NJ), pp. xii+260.
- 368 3. Atiyah MF, Hitchin NJ, Drinfeld VG, Manin YI (1978) Construction of instantons. *Phys. Lett. A*  
 369 65(3):185–187.
- 370 4. Eriksson N, Ranestad K, Sturmels B, Sullivant S (2005) Phylogenetic algebraic geometry in  
 371 *Projective varieties with unexpected properties*. (Walter de Gruyter, Berlin), pp. 237–255.
- 372 5. Kollar J (1987) The structure of algebraic threefolds: an introduction to Mori's program. *Bull.  
 373 Amer. Math. Soc. (N.S.)* 17(2):211–273.
- 374 6. Kollar J, Mori S (1998) *Birational geometry of algebraic varieties*, Cambridge Tracts in Mathematics. (Cambridge University Press, Cambridge) Vol. 134, pp. viii+254.
- 375 7. Del Pezzo P (1887) Sulla superficie dell' $n^{\text{mo}}$  ordine immerse nello spazio ad  $n$  dimensioni.  
 376 *Rend. del Circolo Mat. di Palermo* 1:241–255.
- 377 8. Fano G (1947) Nuove ricerche sulle varietà algebriche a tre dimensioni a curve-sezioni canon-  
 378 iche. *Pont. Acad. Sci. Comment.* 11:635–720.
- 379 9. Iskovskih VA (1977) Fano threefolds. I. *Izv. Akad. Nauk SSSR Ser. Mat.* 41(3):516–562, 717.
- 380 10. Iskovskih VA (1978) Fano threefolds. II. *Izv. Akad. Nauk SSSR Ser. Mat.* 42(3):506–549.
- 381 11. Iskovskih VA (1979) Anticanonical models of three-dimensional algebraic varieties in *Current  
 382 problems in mathematics, Vol. 12 (Russian)*. (VINITI, Moscow), pp. 59–157, 239 (loose  
 383 errata).
- 384 12. Mori S, Mukai S (1981/82) Classification of Fano 3-folds with  $B_2 \geq 2$ . *Manuscripta Math.*  
 385 36(2):147–162.
- 386 13. Mori S, Mukai S (2003) Erratum: “Classification of Fano 3-folds with  $B_2 \geq 2$ ”. *Manuscripta  
 387 Math.* 110(3):407.
- 388 14. Candelas P, de la Ossa XC, Green PS, Parkes L (1991) A pair of Calabi-Yau manifolds as an  
 389 exactly soluble superconformal theory. *Nuclear Phys. B* 359(1):21–74.
- 390 15. Greene BR, Plesser MR (1990) Duality in Calabi-Yau moduli space. *Nuclear Phys. B*  
 391 338(1):15–37.
- 392 16. Hori K, Vafa C (2000) Mirror symmetry. [arXiv:hep-th/0002222](https://arxiv.org/abs/hep-th/0002222).
- 393 17. Cox DA, Katz S (1999) *Mirror symmetry and algebraic geometry*, Mathematical Surveys and  
 394 Monographs. (American Mathematical Society, Providence, RI) Vol. 68, pp. xxii+469.
- 395 18. Coates T, Corti A, Galkin S, Golyshev V, Kasprzyk AM (2013) Mirror symmetry and Fano  
 396 manifolds in *European Congress of Mathematics*. (Eur. Math. Soc., Zürich), pp. 285–300.
- 397 19. Davies A, et al. (2021) Advancing mathematics by guiding human intuition with AI. *Nature*  
 398 600:70–74.
- 399 20. Kreuzer M, Skarke H (2000) Complete classification of reflexive polyhedra in four dimensions.  
 400 *Adv. Theor. Math. Phys.* 4(6):1209–1230.
- 401 21. Conway JH, Curtis RT, Norton SP, Parker RA, Wilson RA (1985) *ATLAS of finite groups*. (Ox-  
 402 ford University Press, Eynsham), pp. xxiv+252. Maximal subgroups and ordinary characters  
 403 for simple groups, With computational assistance from J. G. Thackray.
- 404 22. Cremona J (2016) The L-functions and modular forms database project. *Found. Comput.  
 405 Math.* 16(6):1541–1553.
- 406 23. Adams J, et al. (2016) Atlas of Lie groups and representations (online). <http://www.liegroups.org>.
- 407 24. Coates T, Kasprzyk AM (2022) Databases of quantum periods for Fano manifolds. *Scientific  
 408 Data* 9(1):163.
- 409 25. Coates T, Corti A, Galkin S, Kasprzyk AM (2016) Quantum periods for 3-dimensional Fano  
 410 manifolds. *Geom. Topol.* 20(1):103–256.
- 411 26. Reid M (1980) Canonical 3-folds in *Journées de Géométrie Algébrique d'Angers, Juillet  
 412 1979/Algebraic Geometry, Angers, 1979*. (Sijthoff & Noordhoff, Alphen aan den Rijn—  
 413 Germantown, Md.), pp. 273–310.
- 414 27. Reid M (1987) Young person's guide to canonical singularities in *Algebraic geometry, Bow-  
 415 doin, 1985 (Brunswick, Maine, 1985)*, Proc. Sympos. Pure Math. (Amer. Math. Soc., Provi-  
 416 dence, RI) Vol. 46, pp. 345–414.
- 417 28. Kasprzyk AM (2013) Classifying terminal weighted projective space. [arXiv:1304.3029](https://arxiv.org/abs/1304.3029)  
 418 [math.AG].
- 419 29. Kasprzyk AM (2009) Bounds on fake weighted projective space. *Kodai Math. J.* 32(2):197–  
 420 208.
- 421 30. Kasprzyk AM (2006) Toric Fano three-folds with terminal singularities. *Tohoku Math. J.* (2)  
 422 58(1):101–121.
- 423 31. Coates T, Kasprzyk AM, Veneziale S (2022) A dataset of 150000 terminal weighted projective  
 424 spaces (*Zenodo* <https://doi.org/10.5281/zenodo.5790079>).
- 425 32. Bosma W, Cannon J, Playoust C (1997) The Magma algebra system. I. The user language.  
 426 *J. Symbolic Comput.* 24(3-4):235–265. Computational algebra and number theory (London,  
 427 1993).
- 428 33. European Organization For Nuclear Research, OpenAIRE (2013) Zenodo.
- 429 34. Fulton W (1993) *Introduction to toric varieties*, Annals of Mathematics Studies. (Princeton  
 430 University Press, Princeton, NJ) Vol. 131, pp. xii+157. The William H. Roever Lectures in  
 431 Geometry.
- 432 35. Kreuzer M, Skarke H (2004) PALP: a package for analysing lattice polytopes with applications  
 433 to toric geometry. *Comput. Phys. Comm.* 157(1):87–106.
- 434 36. Grinis R, Kasprzyk AM (2013) Normal forms of convex lattice polytopes. [arXiv:1301.6641](https://arxiv.org/abs/1301.6641)  
 435 [math.CO].
- 436 37. Coates T, Kasprzyk AM, Veneziale S (2022) A dataset of 200000 terminal toric varieties of  
 437 Picard rank 2 (*Zenodo* <https://doi.org/10.5281/zenodo.5790096>).



## **Supporting Information for**

### **Machine Learning the Dimension of a Fano Variety**

**Tom Coates, Alexander M. Kasprzyk and Sara Veneziale**

**Sara Veneziale**  
E-mail: [s.veneziale21@imperial.ac.uk](mailto:s.veneziale21@imperial.ac.uk)

**This PDF file includes:**

Supporting text  
Figs. S1 to S13  
Tables S1 to S4  
SI References

## Supporting Information Text

### 1. Mathematical background

We begin with an introduction to weighted projective spaces and toric varieties, aimed at non-specialists.

**Projective space and weighted projective space.** The fundamental example of a Fano variety is two-dimensional projective space  $\mathbb{P}^2$ . This is a quotient of  $\mathbb{C}^3 \setminus \{0\}$  by the group  $\mathbb{C}^\times$ , where the action of  $\lambda \in \mathbb{C}^\times$  identifies the points  $(x, y, z)$  and  $(\lambda x, \lambda y, \lambda z)$  in  $\mathbb{C}^3 \setminus \{0\}$ . The variety  $\mathbb{P}^2$  is smooth: we can see this by covering it with three open sets  $U_x, U_y, U_z$  that are each isomorphic to the plane  $\mathbb{C}^2$ :

$$\begin{aligned} U_x &= \{(1, Y, Z)\} && \text{given by rescaling } x \text{ to 1} \\ U_y &= \{(X, 1, Z)\} && \text{given by rescaling } y \text{ to 1} \\ U_z &= \{(X, Y, 1)\} && \text{given by rescaling } z \text{ to 1} \end{aligned}$$

Here, for example, in the case  $U_x$  we take  $x \neq 0$  and set  $Y = y/x, Z = z/x$ .

The projective space  $\mathbb{P}^2$  is smooth, but there are closely related Fano varieties called weighted projective spaces (1, 2) that have singularities. For example, consider the weighted projective plane  $\mathbb{P}(1, 2, 3)$ : this is the quotient of  $\mathbb{C}^3 \setminus \{0\}$  by  $\mathbb{C}^\times$ , where the action of  $\lambda \in \mathbb{C}^\times$  identifies the points  $(x, y, z)$  and  $(\lambda x, \lambda^2 y, \lambda^3 z)$ . Let us write

$$\mu_n = \{e^{2\pi k i/n} \mid k \in \mathbb{Z}\}$$

for the group of  $n$ th roots of unity. The variety  $\mathbb{P}(1, 2, 3)$  is once again covered by open sets

$$\begin{aligned} U_x &= \{(1, Y, Z)\} && \text{given by rescaling } x \text{ to 1} \\ U_y &= \{(X, 1, Z)\} && \text{given by rescaling } y \text{ to 1} \\ U_z &= \{(X, Y, 1)\} && \text{given by rescaling } z \text{ to 1} \end{aligned}$$

but this time we have  $U_x \cong \mathbb{C}^2$ ,  $U_y \cong \mathbb{C}^2/\mu_2$ , and  $U_z \cong \mathbb{C}^2/\mu_3$ . This is because, for example, when we choose  $\lambda \in \mathbb{C}^\times$  to rescale  $(x, y, z)$  with  $z \neq 0$  to  $(X, Y, 1)$ , there are three possible choices for  $\lambda$  and they differ by the action of  $\mu_3$ . In particular this lets us see that  $\mathbb{P}(1, 2, 3)$  is singular. For example, functions on the chart  $U_y \cong \mathbb{C}^2/\mu_2$  are polynomials in  $X$  and  $Z$  that are invariant under  $X \mapsto -X, Z \mapsto -Z$ , or in other words

$$\begin{aligned} U_y &= \text{Spec } \mathbb{C}[X^2, XZ, Z^2] \\ &= \text{Spec } \mathbb{C}[a, b, c]/(ac - b^2) \end{aligned}$$

Thus the chart  $U_y$  is the solution set for the equation  $ac - b^2 = 0$ , as pictured in Figure S1a. Similarly, the chart  $U_z \cong \mathbb{C}^2/\mu_3$  can be written as

$$\begin{aligned} U_z &= \text{Spec } \mathbb{C}[X^3, XY, Y^3] \\ &= \text{Spec } \mathbb{C}[a, b, c]/(ac - b^3) \end{aligned}$$

and is the solution set to the equation  $ac - b^3 = 0$ , as pictured in Figure S1b. The variety  $\mathbb{P}(1, 2, 3)$  has singular points at  $(0, 1, 0) \in U_y$  and  $(0, 0, 1) \in U_z$ , and away from these points it is smooth.

There are weighted projective spaces of any dimension. Let  $a_1, a_2, \dots, a_N$  be positive integers such that any subset of size  $N - 1$  has no common factor, and consider

$$\mathbb{P}(a_1, a_2, \dots, a_N) = (\mathbb{C}^N \setminus \{0\})/\mathbb{C}^\times$$

where the action of  $\lambda \in \mathbb{C}^\times$  identifies the points

$$(x_1, x_2, \dots, x_N) \quad \text{and} \quad (\lambda^{a_1} x_1, \lambda^{a_2} x_2, \dots, \lambda^{a_N} x_N)$$

in  $\mathbb{C}^N \setminus \{0\}$ . The quotient  $\mathbb{P}(a_1, a_2, \dots, a_N)$  is an algebraic variety of dimension  $N - 1$ . A general point of  $\mathbb{P}(a_1, a_2, \dots, a_N)$  is smooth, but there can be singular points. Indeed,  $\mathbb{P}(a_1, a_2, \dots, a_N)$  is covered by  $N$  open sets

$$U_i = \{(X_1, \dots, X_{i-1}, 1, X_{i+1}, \dots, X_N)\} \quad i \in \{1, 2, \dots, N\}$$

given by rescaling  $x_i$  to 1; here we take  $x_i \neq 0$  and set  $X_j = x_j/x_i$ . The chart  $U_i$  is isomorphic to  $\mathbb{C}^{N-1}/\mu_{a_i}$ , where  $\mu_{a_i}$  acts on  $\mathbb{C}^{N-1}$  with weights  $a_j, j \neq i$ . In Reid's notation, this is the cyclic quotient singularity  $\frac{1}{a_i}(a_1, \dots, \hat{a}_i, \dots, a_N)$ ; it is smooth if and only if  $a_i = 1$ .

The topology of weighted projective space is very simple, with

$$H^k(\mathbb{P}(a_1, a_2, \dots, a_N); \mathbb{Q}) = \begin{cases} \mathbb{Q} & \text{if } 0 \leq k \leq 2N - 2 \text{ and } k \text{ is even;} \\ 0 & \text{otherwise.} \end{cases}$$

Hence every weighted projective space has second Betti number  $b_2 = 1$ . There is a closed formula (3, Proposition D.9) for the regularized quantum period of  $X = \mathbb{P}(a_1, a_2, \dots, a_N)$ :

$$\widehat{G}_X(t) = \sum_{k=0}^{\infty} \frac{(ak)!}{(a_1 k)!(a_2 k)! \cdots (a_N k)!} t^{ak} \quad [1]$$

where  $a = a_1 + a_2 + \cdots + a_N$ .

**Toric varieties of Picard rank 2.** As well as weighted projective spaces, which are quotients of  $\mathbb{C}^N \setminus \{0\}$  by an action of  $\mathbb{C}^\times$ , we will consider varieties that arise as quotients of  $\mathbb{C}^N \setminus S$  by  $(\mathbb{C}^\times)^2$ , where  $S$  is a union of linear subspaces. These are examples of *toric varieties* (4, 5). Specifically, consider a matrix

$$\begin{pmatrix} a_1 & a_2 & \cdots & a_N \\ b_1 & b_2 & \cdots & b_N \end{pmatrix} \quad [2]$$

with non-negative integer entries and no zero columns. This defines an action of  $(\mathbb{C}^\times)^2$  on  $\mathbb{C}^N$ , where  $(\lambda, \mu) \in (\mathbb{C}^\times)^2$  identifies the points

$$(x_1, x_2, \dots, x_N) \quad \text{and} \quad (\lambda^{a_1} \mu^{b_1} x_1, \lambda^{a_2} \mu^{b_2} x_2, \dots, \lambda^{a_N} \mu^{b_N} x_N)$$

in  $\mathbb{C}^N$ . Set  $a = a_1 + a_2 + \dots + a_N$  and  $b = b_1 + b_2 + \dots + b_N$ , and suppose that  $(a, b)$  is not a scalar multiple of  $(a_i, b_i)$  for any  $i$ . This determines linear subspaces

$$\begin{aligned} S_+ &= \{(x_1, x_2, \dots, x_N) \mid x_i = 0 \text{ if } b_i/a_i < b/a\} \\ S_- &= \{(x_1, x_2, \dots, x_N) \mid x_i = 0 \text{ if } b_i/a_i > b/a\} \end{aligned}$$

of  $\mathbb{C}^N$ , and we consider the quotient

$$X = (\mathbb{C}^N \setminus S) / (\mathbb{C}^\times)^2 \quad [3]$$

where  $S = S_+ \cup S_-$ . See e.g. (6, §A.5).

These quotients behave in many ways like weighted projective spaces. Indeed, if we take the weight matrix [2] to be

$$\begin{pmatrix} a_1 & a_2 & \cdots & a_N & 0 \\ 0 & 0 & \cdots & 0 & 1 \end{pmatrix}$$

then  $X$  coincides with  $\mathbb{P}(a_1, a_2, \dots, a_N)$ . We will consider only weight matrices such that the subspaces  $S_+$  and  $S_-$  both have dimension two or more; this implies that the second Betti number  $b_2(X) = 2$ , and hence  $X$  is not a weighted projective space. We will refer to such quotients [3] as *toric varieties of Picard rank two*, because general theory implies that the Picard lattice of  $X$  has rank two. The dimension of  $X$  is  $N - 2$ . As for weighted projective spaces, toric varieties of Picard rank two can have singular points, the precise form of which is determined by the weights [2]. There is also a closed formula (3, Proposition C.2) for the regularized quantum period. Let  $C$  denote the cone in  $\mathbb{R}^2$  defined by the equations  $a_i x + b_i y \geq 0$ ,  $i \in \{1, 2, \dots, N\}$ . Then

$$\widehat{G}_X(t) = \sum_{(k,l) \in \mathbb{Z}^2 \cap C} \frac{(ak + bl)!}{(a_1 k + b_1 l)!(a_2 k + b_2 l)! \cdots (a_N k + b_N l)!} t^{ak + bl} \quad [4]$$

**Classification results.** Weighted projective spaces with at worst terminal singularities have been classified in dimensions up to four; see Table S1 for a summary. Fano toric varieties with at worst terminal singularities have been classified in dimension three (7); 35 of them have quotient singularities and Picard rank two. There is no known classification of Fano toric varieties with at worst terminal singularities in higher dimension, even when the Picard rank is two.

## 2. Data analysis

**Weighted projective space.** As discussed in the main text, we first computed an initial segment  $(c_0, c_1, \dots, c_m)$  of the regularized quantum period for all the examples in the sample of 150 000 terminal weighted projective spaces, with  $m \approx 100 000$ . We then considered  $\{\log c_d\}_{d \in S}$  where  $S = \{d \in \mathbb{Z}_{\geq 0} \mid c_d \neq 0\}$ . To reduce dimension we fitted a linear model to the set  $\{(d, \log c_d) \mid d \in S\}$  and used the slope and intercept of this model as features. The linear fit produces a close approximation of the data. Figure S2 shows the distribution of the standard errors for the slope and the  $y$ -intercept: the errors for the slope are between  $3.9 \times 10^{-8}$  and  $1.4 \times 10^{-5}$ , and the errors for the  $y$ -intercept are between 0.0022 and 0.82. As we will see below, the standard error for the  $y$ -intercept is a good proxy for the accuracy of the linear model. This accuracy decreases as the dimension grows – see Figure S2c – but we will see below that this does not affect the accuracy of the machine learning classification.

**Toric varieties of Picard rank 2.** We fitted a linear model to the set  $\{(d, \log c_d) \mid d \in S\}$  where  $S = \{d \in \mathbb{Z}_{\geq 0} \mid c_d \neq 0\}$ , and used the slope and intercept of this linear model as features. The distribution of standard errors for the slope and  $y$ -intercept of the linear model are shown in Figure S4. The standard errors for the slope are small compared to the range of slopes, but in many cases the standard error for the  $y$ -intercept is relatively large. As Figure S5 illustrates, discarding data points where the standard error  $s_{\text{int}}$  for the  $y$ -intercept exceeds some threshold reduces apparent noise. As discussed in the main text, we believe that this reflects inaccuracies in the linear regression caused by oscillatory behaviour in the initial terms of the quantum period sequence. See also Figure 6 in the main text.

**Example 1.** Let us consider in more detail the toric variety from Example 3 in the main text. In Figure S3 we plot  $\log c_d$  along with its linear approximation. Figure S3a shows only the first 250 terms, whilst Figure S3b shows the interval between the 1000th and the 1250th term. We see considerable deviation from the linear approximation amongst the first 250 terms; the deviation reduces for larger  $d$ .

### 3. Applying machine learning

We performed our experiments using scikit-learn (8), a standard machine learning library for Python. We used scikit-learn v0.24.1 and Python v3.8.8; the code used to perform this analysis is available from Bitbucket under an MIT license (9).

**Weighted projective space.** We excluded dimensions one and two from the analysis, since there is only one weighted projective space in each case (namely  $\mathbb{P}^1$  and  $\mathbb{P}^2$ ). Therefore we have a dataset of 149 998 slope-intercept pairs, labelled by the dimension which varies between three and ten. We standardised the features, by translating the means to zero and scaling to unit variance, and applied a Support Vector Machine (SVM) with linear kernel and regularisation parameter  $C = 10$ . By looking at different train–test splits we obtained the learning curves shown in Figure S6. The figure displays the mean accuracies for both training and validation data obtained by performing five random test-train splits each time: the shaded areas around the lines correspond to the  $1\sigma$  region, where  $\sigma$  denotes the standard deviation. Using 10% (or more) of the data for training we obtained an accuracy of 99.99%. In Figure S7 we plot the decision boundaries computed by the SVM between neighbouring dimension classes.

**Toric varieties of Picard rank 2.** In light of the discussion above, we restricted attention to toric varieties with Picard rank two such that the  $y$ -intercept standard error  $s_{\text{int}}$  is less than 0.3. We also excluded dimension two from the analysis, since in this case there are only two varieties (namely,  $\mathbb{P}^1 \times \mathbb{P}^1$  and the Hirzebruch surface  $\mathbb{F}_1$ ). The resulting dataset contains 67 443 slope-intercept pairs, labelled by dimension; the dimension varies between three and ten, as shown in Table S2.

**Support Vector Machine.** We used a linear SVM with regularisation parameter  $C = 50$ . By considering different train–test splits we obtained the learning curves shown in Figure S8, where the means and the standard deviations were obtained by performing five random samples for each split. Note that the model did not overfit. We obtained a validation accuracy of 88.20% using 70% of the data for training. Figure S9 shows the decision boundaries computed by the SVM between neighbouring dimension classes. Figure S10 shows the confusion matrices for the same train–test split.

**Random Forest Classifier.** We used a Random Forest Classifier (RFC) with 1500 estimators and the same features (slope and  $y$ -intercept for the linear model). By considering different train–test splits we obtained the learning curves shown in Figure S11; note again that the model did not overfit. Using 70% of the data for training, the RFC gave a validation accuracy of 89.39%. Figure S12 shows confusion matrices for the same train–test split.

**Neural Network.** Neural networks do not handle unbalanced datasets well. We therefore removed those terminal weighted projective spaces with dimensions three, four, and five from our dataset: see Table S2. We trained a Multilayer Perceptron (MLP) classifier on the same features, using an MLP with three hidden layers (10, 30, 10), Adam optimiser (10), and rectified linear activation function (11). Different train–test splits produced the learning curve in Figure S13; again the model did not overfit. Using 70% of the data for training, the MLP gave a validation accuracy of 89.03%. One could further balance the dataset, by randomly undersampling so that there are the same number of representatives in each dimension (8244 representatives: see Table S2). This resulted in a slight decrease in accuracy: the better balance was outweighed by loss of data caused by undersampling.

The validation accuracies of the SVM, RFC, and MLP on the same data set ( $s_{\text{int}} < 0.3$ , dimension between six and ten) and for the same train–test split are compared in Table S3, and their confusion matrices are shown in Table S4. All models performed well, with the RFC slightly more accurate than the SVM and the MLP slightly more accurate still. Note that misclassified examples are generally in higher dimension, which is consistent with the idea that misclassification is due to convergence-related noise.

### 4. Rigorous asymptotics for the regularized quantum period

**Weighted projective space.** The following result implies Theorem 5 in the main text.

**Theorem 2** (see Theorem 5 in the main text). *Let  $X$  denote the weighted projective space  $\mathbb{P}(a_1, \dots, a_N)$ , so that the dimension of  $X$  is  $N - 1$ . Let  $c_d$  denote the coefficient of  $t^d$  in the regularised quantum period  $\widehat{G}_X(t)$  given in [1]. Let  $a = a_1 + \dots + a_N$ . Then  $c_d = 0$  unless  $d$  is divisible by  $a$ , and*

$$\log c_{ka} \sim ka \left[ \log a - \frac{1}{a} \sum_{i=1}^N a_i \log a_i \right] - \frac{\dim X}{2} \log(ka) + \frac{1 + \dim X}{2} \log a - \frac{\dim X}{2} \log(2\pi) - \frac{1}{2} \sum_{i=1}^N \log a_i$$

That is, non-zero coefficients  $c_d$  satisfy

$$\log c_d \sim Ad - \frac{\dim X}{2} \log d + B$$

as  $d \rightarrow \infty$ , where

$$A = - \sum_{i=1}^N p_i \log p_i \quad B = - \frac{\dim X}{2} \log(2\pi) - \frac{1}{2} \sum_{i=1}^N \log p_i$$

and  $p_i = a_i/a$ .

*Proof.* Combine Stirling's formula

$$n! \sim \sqrt{2\pi n} \left(\frac{n}{e}\right)^n$$

with the closed formula [1] for  $c_{ka}$ . □

**Toric varieties of Picard rank 2.** Consider a toric variety  $X$  of Picard rank two and dimension  $N - 2$ , as in §1, with weight matrix

$$\begin{bmatrix} a_1 & a_2 & a_3 & \cdots & a_N \\ b_1 & b_2 & b_3 & \cdots & b_N \end{bmatrix}$$

Let us move to more invariant notation, writing  $\alpha_i$  for the linear form on  $\mathbb{R}^2$  defined by the transpose of the  $i$ th column of the weight matrix, and  $\alpha = \alpha_1 + \cdots + \alpha_N$ . Equation 4 becomes

$$\widehat{G}_X(t) = \sum_{k \in \mathbb{Z}^2 \cap C} \frac{(\alpha \cdot k)!}{\prod_{i=1}^N (\alpha_i \cdot k)!} t^{\alpha \cdot k}$$

where  $C$  is the cone  $C = \{x \in \mathbb{R}^2 \mid \alpha_i \cdot x \geq 0 \text{ for } i = 1, 2, \dots, N\}$ . As we will see, for  $d \gg 0$  the coefficients

$$\frac{(\alpha \cdot k)!}{\prod_{i=1}^N (\alpha_i \cdot k)!} \quad \text{where } k \in \mathbb{Z}^2 \cap C \text{ and } \alpha \cdot k = d$$

are approximated by a rescaled Gaussian. We begin by finding the mean of that Gaussian, that is, by minimising

$$\prod_{i=1}^N (\alpha_i \cdot k)! \quad \text{where } k \in \mathbb{Z}^2 \cap C \text{ and } \alpha \cdot k = d.$$

For  $k$  in the strict interior of  $C$  with  $\alpha \cdot k = d$ , we have that

$$(\alpha_i \cdot k)! \sim \left(\frac{\alpha \cdot k}{e}\right)^{\alpha \cdot k}$$

as  $d \rightarrow \infty$ .

**Proposition 3.** *The constrained optimisation problem*

$$\min \prod_{i=1}^N (\alpha_i \cdot x)^{\alpha_i \cdot x} \quad \text{subject to } \begin{cases} x \in C \\ \alpha \cdot x = d \end{cases}$$

has a unique solution  $x = x^*$ . Furthermore, setting  $p_i = (\alpha_i \cdot x^*) / (\alpha \cdot x^*)$  we have that the monomial

$$\prod_{i=1}^N p_i^{\alpha_i \cdot k}$$

depends on  $k \in \mathbb{Z}^2$  only via  $\alpha \cdot k$ .

*Proof.* Taking logarithms gives the equivalent problem

$$\min \sum_{i=1}^N (\alpha_i \cdot x) \log(\alpha_i \cdot x) \quad \text{subject to } \begin{cases} x \in C \\ \alpha \cdot x = d \end{cases} \quad [5]$$

The objective function  $\sum_{i=1}^N (\alpha_i \cdot x) \log(\alpha_i \cdot x)$  here is the pullback to  $\mathbb{R}^2$  of the function

$$f(x_1, \dots, x_N) = \sum_{i=1}^N x_i \log x_i$$

along the linear embedding  $\varphi : \mathbb{R}^2 \rightarrow \mathbb{R}^N$  given by  $(\alpha_1, \dots, \alpha_N)$ . Note that  $C$  is the preimage under  $\varphi$  of the positive orthant  $\mathbb{R}_+^N$ , so we need to minimise  $f$  on the intersection of the simplex  $x_1 + \cdots + x_N = d$ ,  $(x_1, \dots, x_N) \in \mathbb{R}_+^N$  with the image of  $\varphi$ . The function  $f$  is convex and decreases as we move away from the boundary of the simplex, so the minimisation problem in Equation 5 has a unique solution  $x^*$  and this lies in the strict interior of  $C$ . We can therefore find the minimum  $x^*$  using the method of Lagrange multipliers, by solving

$$\sum_{i=1}^N \alpha_i \log(\alpha_i \cdot x) + \alpha = \lambda \alpha \quad [6]$$

for  $\lambda \in \mathbb{R}$  and  $x$  in the interior of  $C$  with  $\alpha \cdot x = d$ . Thus

$$\sum_{i=1}^N \alpha_i \log(\alpha_i \cdot x^*) = (\lambda - 1)\alpha$$

and, evaluating on  $k \in \mathbb{Z}^2$  and exponentiating, we see that

$$\prod_{i=1}^N (\alpha_i \cdot x^*)^{\alpha_i \cdot k}$$

depends only on  $\alpha \cdot k$ . The result follows.  $\square$

Given a solution  $x^*$  to Equation 6, any positive scalar multiple of  $x^*$  also satisfies Equation 6, with a different value of  $\lambda$  and a different value of  $d$ . Thus the solutions  $x^*$ , as  $d$  varies, lie on a half-line through the origin. The direction vector  $[\mu : \nu] \in \mathbb{P}^1$  of this half-line is the unique solution to the system

$$\begin{aligned} \prod_{i=1}^N (a_i\mu + b_i\nu)^{a_i b} &= \prod_{i=1}^N (a_i\mu + b_i\nu)^{b_i a} \\ \begin{pmatrix} \mu \\ \nu \end{pmatrix} &\in C \end{aligned} \tag{7}$$

Note that the first equation here is homogeneous in  $\mu$  and  $\nu$ ; it is equivalent to Equation 6, by exponentiating and then eliminating  $\lambda$ . Any two solutions  $x^*$ , for different values of  $d$ , differ by rescaling, and the quantities  $p_i$  in Proposition 3 are invariant under this rescaling. They also satisfy  $p_1 + \dots + p_N = 1$ .

We use the following result, known in the literature as the “local theorem” (12), to approximate multinomial coefficients.

**Local Theorem.** *For  $p_1, \dots, p_n \in [0, 1]$  such that  $p_1 + \dots + p_n = 1$ , the ratio*

$$d^{\frac{n-1}{2}} \binom{d}{k_1 \dots k_n} \prod_{i=1}^n p_i^{k_i} : \frac{\exp(-\frac{1}{2} \sum_{i=1}^n q_i x_i^2)}{(2\pi)^{\frac{n-1}{2}} \sqrt{p_1 \dots p_n}} \rightarrow 1$$

as  $d \rightarrow \infty$ , uniformly in all  $k_i$ 's, where

$$q_i = 1 - p_i \quad x_i = \frac{k_i - dp_i}{\sqrt{dp_i q_i}}$$

and the  $x_i$  lie in bounded intervals.

Let  $B_r$  denote the ball of radius  $r$  about  $x^* \in \mathbb{R}^2$ . Fix  $R > 0$ . We apply the Local Theorem with  $k_i = \alpha_i \cdot k$  and  $p_i = (\alpha_i \cdot x^*)/(\alpha \cdot x^*)$ , where  $k \in \mathbb{Z}^2 \cap C$  satisfies  $\alpha \cdot k = d$  and  $k \in B_{R\sqrt{d}}$ . Since

$$x_i = \frac{\alpha_i \cdot (k - x^*)}{\sqrt{dp_i q_i}}$$

the assumption that  $k \in B_{R\sqrt{d}}$  ensures that the  $x_i$  remain bounded as  $d \rightarrow \infty$ . Note that, by Proposition 3, the monomial  $\prod_{i=1}^N p_i^{k_i}$  depends on  $k$  only via  $\alpha \cdot k$ , and hence here is independent of  $k$ :

$$\prod_{i=1}^N p_i^{k_i} = \prod_{i=1}^N p_i^{\alpha_i \cdot x^*} = \prod_{i=1}^N p_i^{dp_i}$$

Furthermore

$$\sum_{i=1}^N q_i x_i^2 = \frac{(k - x^*)^T A (k - x^*)}{d}$$

where  $A$  is the positive-definite  $2 \times 2$  matrix given by

$$A = \sum_{i=1}^N \frac{1}{p_i} \alpha_i^T \alpha_i$$

Thus as  $d \rightarrow \infty$ , the ratio

$$\frac{(\alpha \cdot k)!}{\prod_{i=1}^N (\alpha_i \cdot k)!} : \frac{\exp\left(-\frac{1}{2d}(k - x^*)^T A (k - x^*)\right)}{(2\pi d)^{\frac{N-1}{2}} \prod_{i=1}^N p_i^{dp_i + \frac{1}{2}}} \rightarrow 1 \tag{8}$$

for all  $k \in \mathbb{Z}^2 \cap C \cap B_{R\sqrt{d}}$  such that  $\alpha \cdot k = d$ .

**Theorem 4** (which is Theorem 6 in the main text). *Let  $X$  be a toric variety of Picard rank two and dimension  $N - 2$ , as in §1, with weight matrix*

$$\begin{bmatrix} a_1 & a_2 & a_3 & \cdots & a_N \\ b_1 & b_2 & b_3 & \cdots & b_N \end{bmatrix}$$

*Let  $a = a_1 + \cdots + a_N$  and  $b = b_1 + \cdots + b_N$ , and let  $[\mu : \nu] \in \mathbb{P}^1$  be the unique solution to Equation 7. Let  $c_d$  denote the coefficient of  $t^d$  in the regularised quantum period  $\widehat{G}_X(t)$ . Then non-zero coefficients  $c_d$  satisfy*

$$\log c_d \sim Ad - \frac{\dim X}{2} \log d + B$$

as  $d \rightarrow \infty$ , where

$$A = -\sum_{i=1}^N p_i \log p_i$$

$$B = -\frac{\dim X}{2} \log(2\pi) - \frac{1}{2} \sum_{i=1}^N \log p_i - \frac{1}{2} \log \left( \sum_{i=1}^N \frac{(a_i b - b_i a)^2}{\ell^2 p_i} \right)$$

$$\text{and } p_i = \frac{\mu a_i + \nu b_i}{\mu a + \nu b}.$$

*Proof.* We need to estimate

$$c_d = \sum_{\substack{k \in \mathbb{Z}^2 \cap C \\ \text{with } \alpha \cdot k = d}} \frac{(\alpha \cdot k)!}{\prod_{i=1}^N (\alpha_i \cdot k)!}$$

Consider first the summands with  $k \in \mathbb{Z}^2 \cap C$  such that  $\alpha \cdot k = d$  and  $k \notin B_{R\sqrt{d}}$ . For  $d$  sufficiently large, each such summand is bounded by  $cd^{-\frac{1+\dim X}{2}}$  for some constant  $c$  – see Equation 8. Since the number of such summands grows linearly with  $d$ , in the limit  $d \rightarrow \infty$  the contribution to  $c_d$  from  $k \notin B_{R\sqrt{d}}$  vanishes.

As  $d \rightarrow \infty$ , therefore

$$c_d \sim \frac{1}{(2\pi d)^{\frac{N-1}{2}} \prod_{i=1}^N p_i^{dp_i + \frac{1}{2}}} \sum_{\substack{k \in \mathbb{Z}^2 \cap C \cap B_{R\sqrt{d}} \\ \text{with } \alpha \cdot k = d}} \exp \left( -\frac{(k - x^*)^T A (k - x^*)}{2d} \right)$$

Writing  $y_k = (k - x^*)/\sqrt{d}$ , considering the sum here as a Riemann sum, and letting  $R \rightarrow \infty$ , we see that

$$c_d \sim \frac{1}{(2\pi d)^{\frac{N-1}{2}} \prod_{i=1}^N p_i^{dp_i + \frac{1}{2}}} \sqrt{d} \int_{y \in L_\alpha} \exp \left( -\frac{1}{2} y^T A y \right) dy$$

where  $L_\alpha$  is the line through the origin given by  $\ker \alpha$  and  $dy$  is the measure on  $L_\alpha$  given by the integer lattice  $\mathbb{Z}^2 \cap L_\alpha \subset L_\alpha$ .

To evaluate the integral, let

$$\alpha^\perp = \frac{1}{\ell} \begin{pmatrix} b \\ -a \end{pmatrix} \quad \text{where } \ell = \gcd\{a, b\}$$

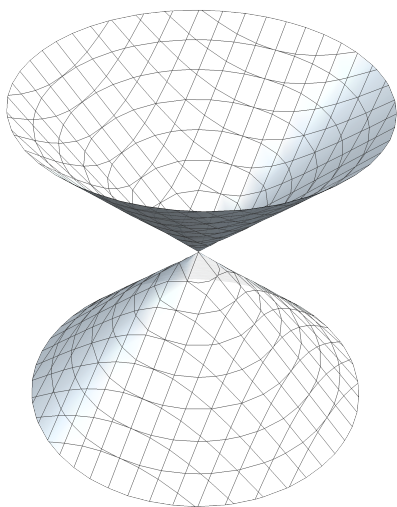
and observe that the pullback of  $dy$  along the map  $\mathbb{R} \rightarrow L_\alpha$  given by  $t \mapsto t\alpha^\perp$  is the standard measure on  $\mathbb{R}$ . Thus

$$\int_{L_\alpha} \exp \left( -\frac{1}{2} y^T A y \right) dy = \int_{-\infty}^{\infty} \exp \left( -\frac{1}{2} \theta x^2 \right) dx = \sqrt{\frac{2\pi}{\theta}}$$

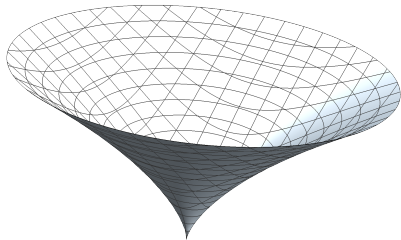
where  $\theta = \sum_{i=1}^N \frac{1}{\ell^2 p_i} (\alpha_i \cdot \alpha^\perp)^2$ , and

$$c_d \sim \frac{1}{(2\pi d)^{\frac{\dim X}{2}} \prod_{i=1}^N p_i^{dp_i + \frac{1}{2}} \sqrt{\theta}}$$

Taking logarithms gives the result.  $\square$



a The real locus in the chart  $U_y$ .



b The real locus in the chart  $U_z$ .

**Fig. S1.** Singular charts on the weighted projective space  $\mathbb{P}(1, 2, 3)$ .

Dimension			
1	2	3	4
$\mathbb{P}^1$	$\mathbb{P}^2$	7 cases see (7)	28 686 cases see (13)

**Table S1.** The classification of weighted projective spaces in low dimensions.

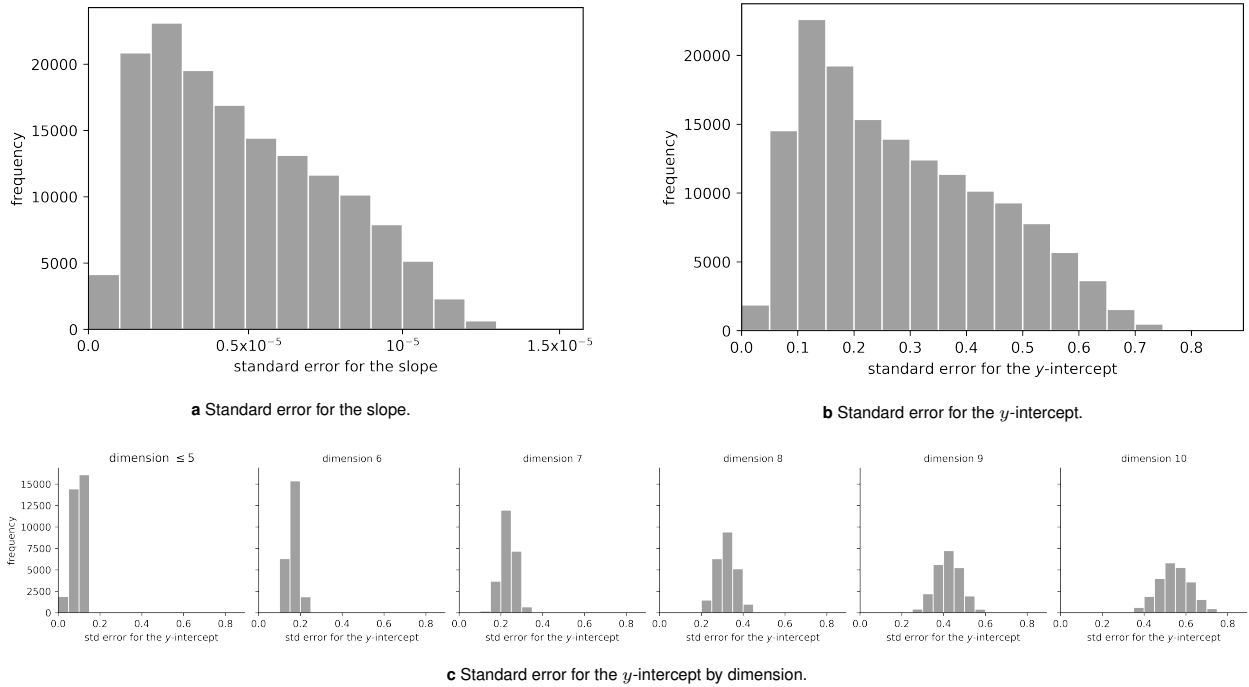


**Fig. S2.** The distribution of standard errors for the slope and  $y$ -intercept from the linear model applied to weighted projective spaces  $X$  with terminal singularities.

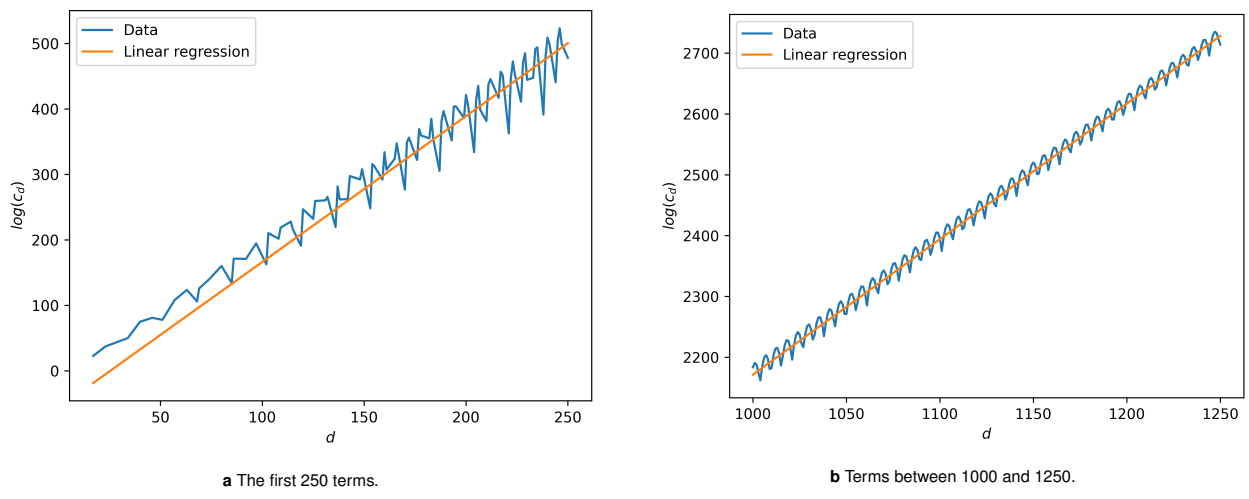
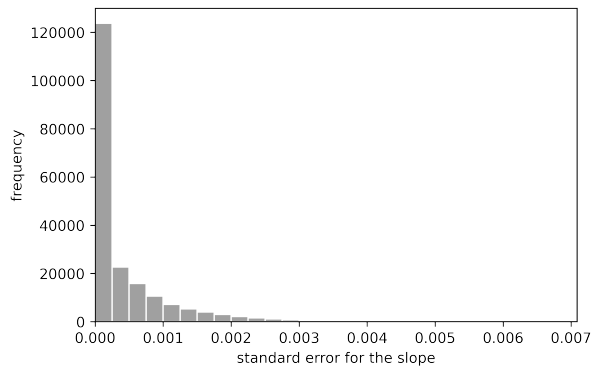
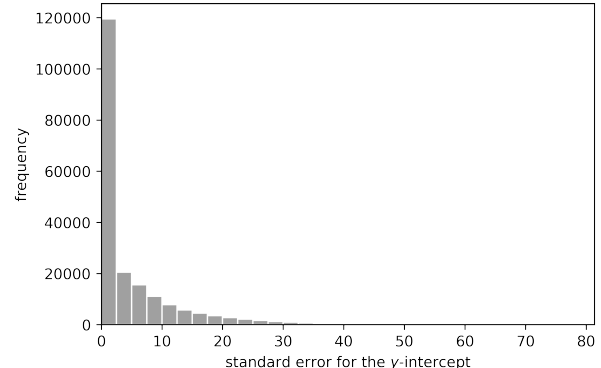


**Fig. S3.** Different sections of the graph of the logarithm of the regularized quantum period sequence for Example 1, together with its linear approximation.

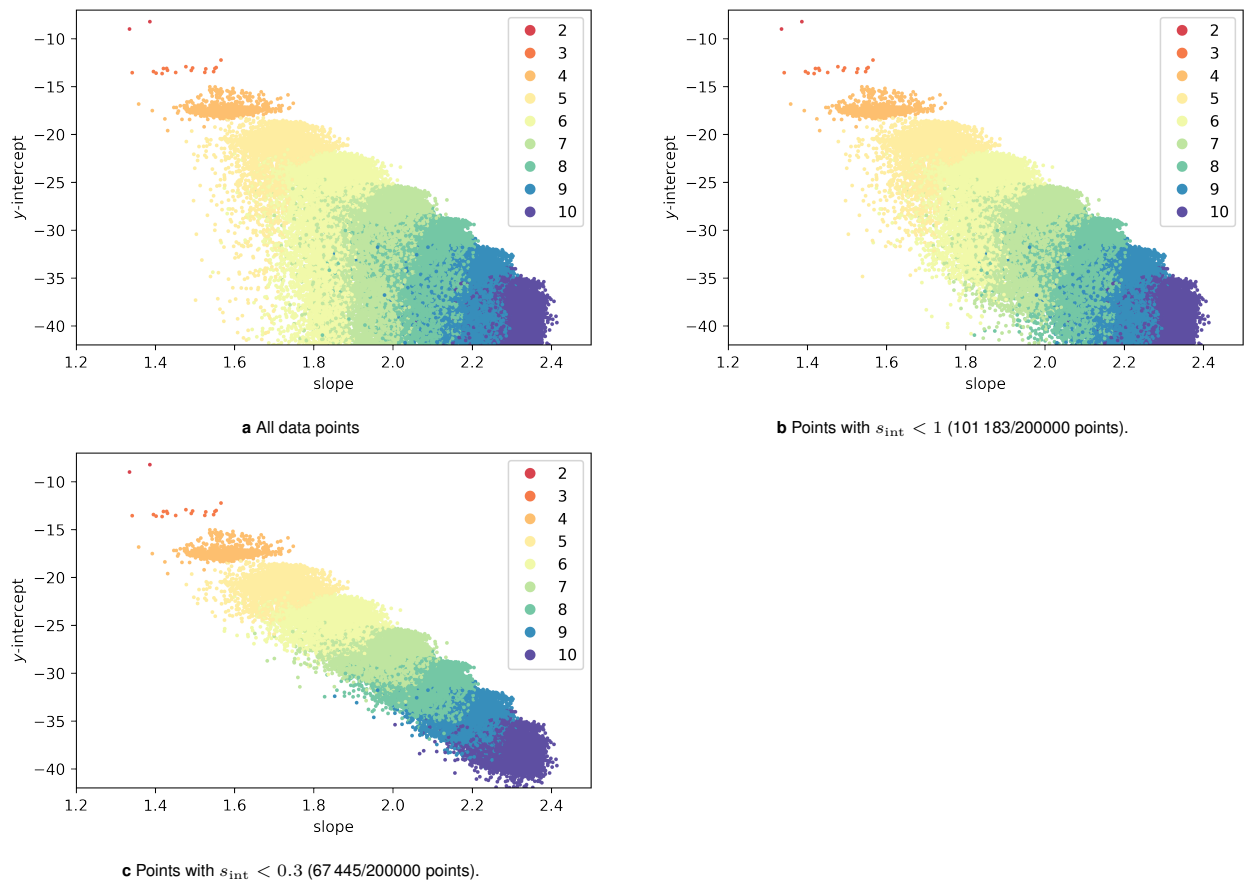


**a** Standard error for the slope.



**b** Standard error for the  $y$ -intercept.

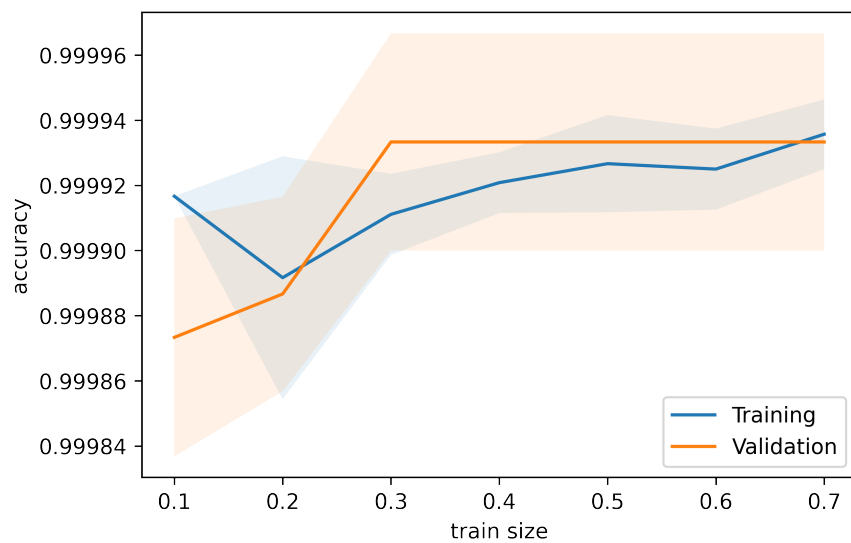
**Fig. S4.** The distribution of standard errors for the slope and  $y$ -intercept from the linear model applied to toric varieties of Picard rank two with terminal singularities.



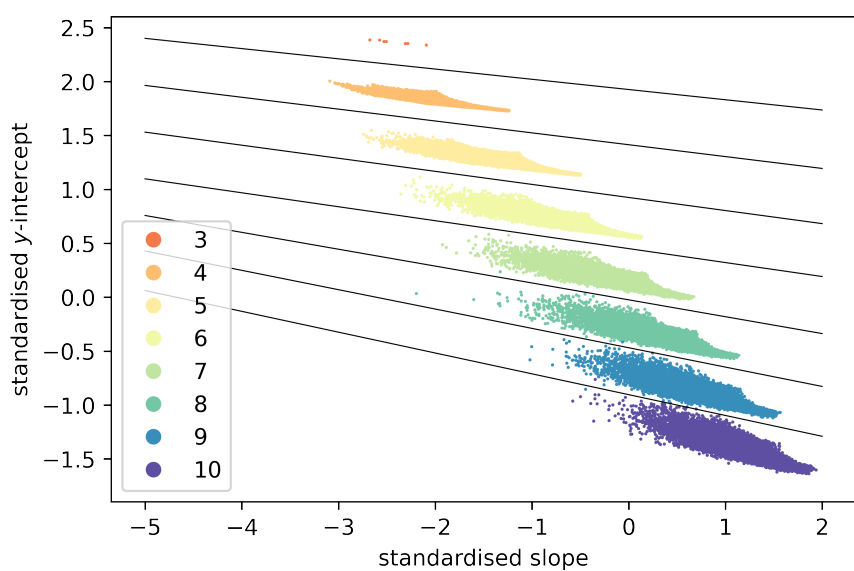
**Fig. S5.** The slopes and  $y$ -intercepts from the linear model applied to toric varieties of Picard rank two, selecting data points according to the standard error  $s_{\text{int}}$  for the  $y$ -intercept. The colour records the dimension of the toric variety.

Rank-two toric varieties with $s_{\text{int}} < 0.3$		
Dimension	Sample size	Percentage
3	17	0.025
4	758	1.124
5	5504	8.161
6	12497	18.530
7	16084	23.848
8	13701	20.315
9	10638	15.773
10	8244	12.224
Total	67443	

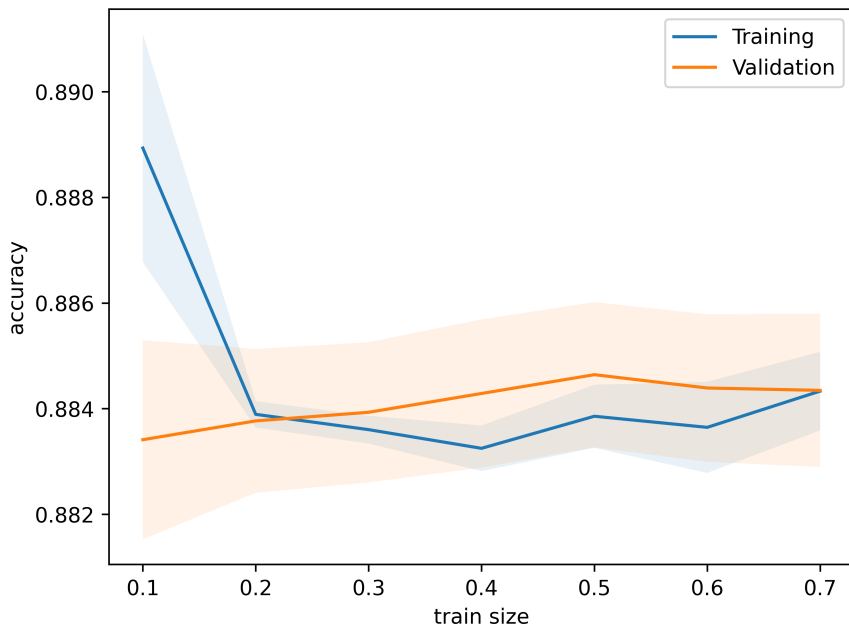
**Table S2.** The number and percentage of toric varieties of Picard rank two with  $s_{\text{int}} < 0.3$  appearing in the sample data, by dimension.



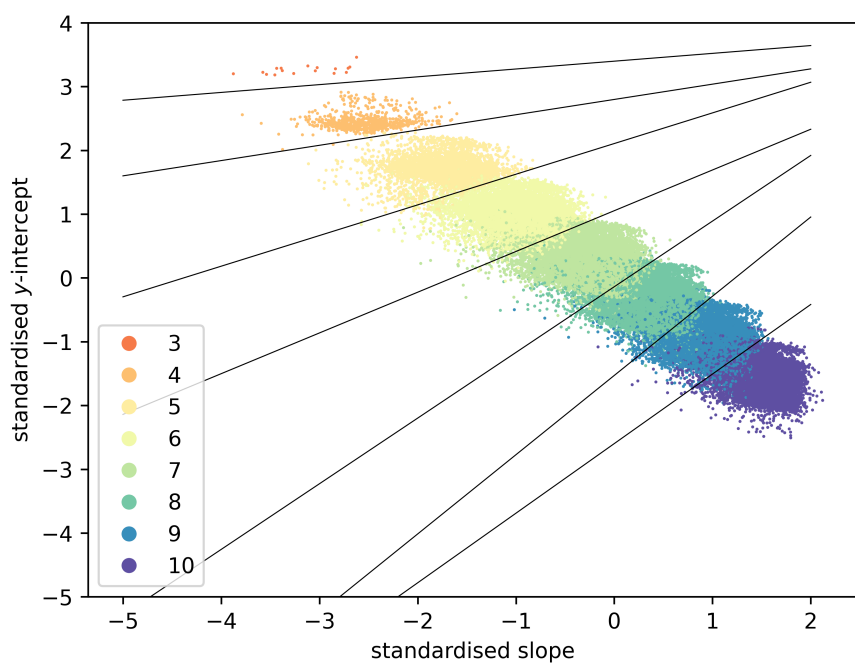
**Fig. S6.** Learning curves for a linear SVM applied to the dataset of terminal weighted projective spaces. The plot shows the means of the training and validation accuracies for five different random train–test splits. The shaded regions correspond to the  $1\sigma$  interval, where  $\sigma$  denotes the standard deviation.



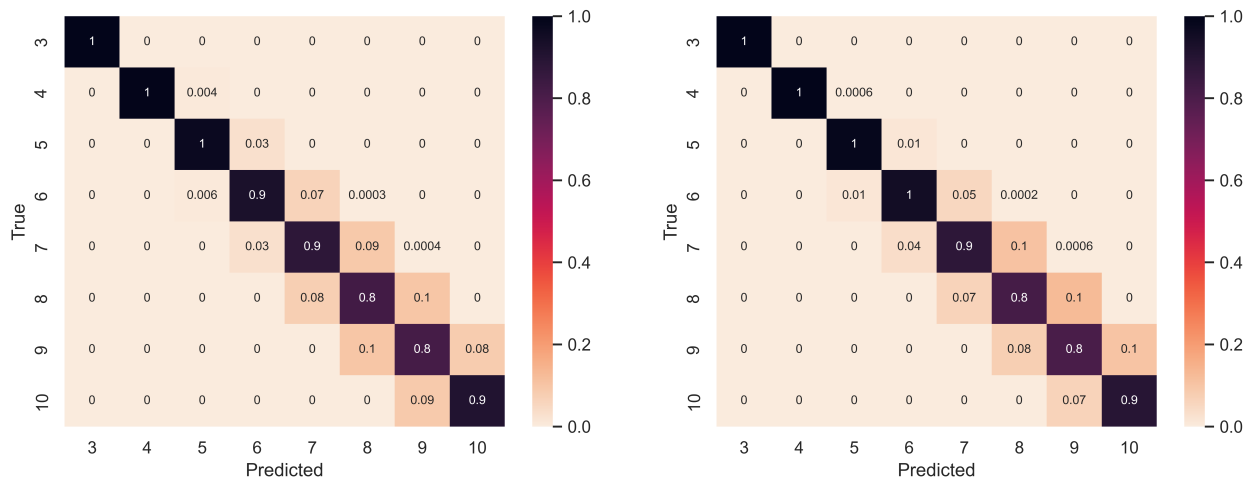
**Fig. S7.** Decision boundaries computed from a linear SVM trained on 70% of the dataset of terminal weighted projective spaces. Note that the data has been standardised.



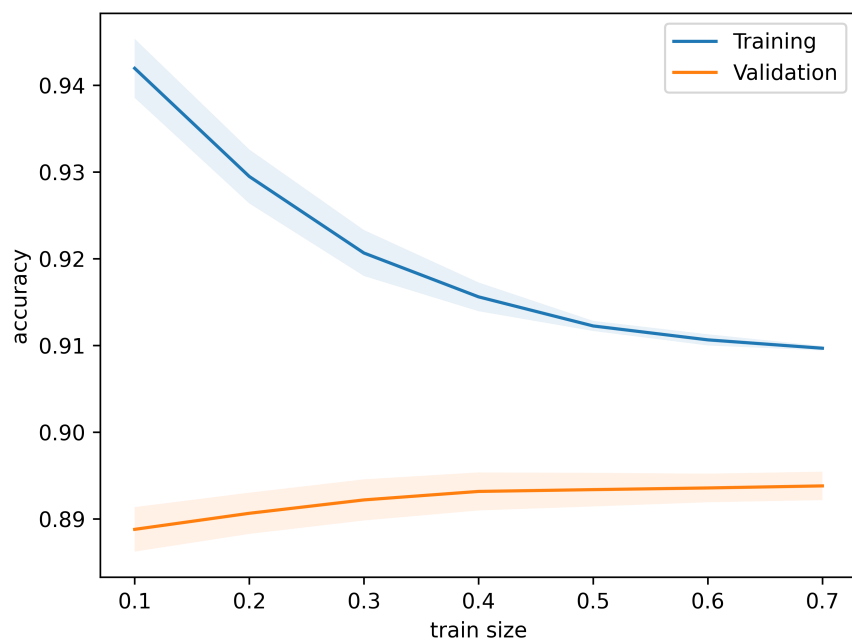
**Fig. S8.** Learning curves for a linear SVM applied to the dataset of toric varieties of Picard rank two. The plot shows the means of the training and validation accuracies for five different random train–test splits. The shaded regions correspond to the  $1\sigma$  interval, where  $\sigma$  denotes the standard deviation.



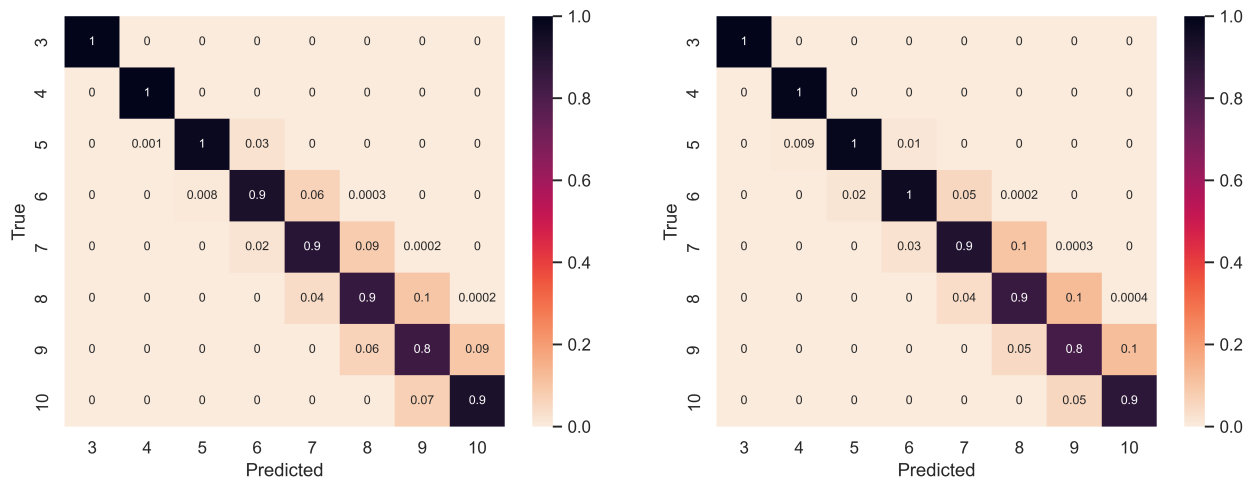
**Fig. S9.** Decision boundaries computed from a linear SVM trained on 70% of the dataset of toric varieties of Picard rank two. Note that the data has been standardised.



**Fig. S10.** Confusion matrices for a linear SVM trained on 70% of the dataset of toric varieties of Picard rank two.



**Fig. S11.** Learning curves for a Random Forest Classifier applied to the dataset of toric varieties of Picard rank two. The plot shows the means of the training and validation accuracies for five different random train–test splits. The shaded regions correspond to the  $1\sigma$  interval, where  $\sigma$  denotes the standard deviation.



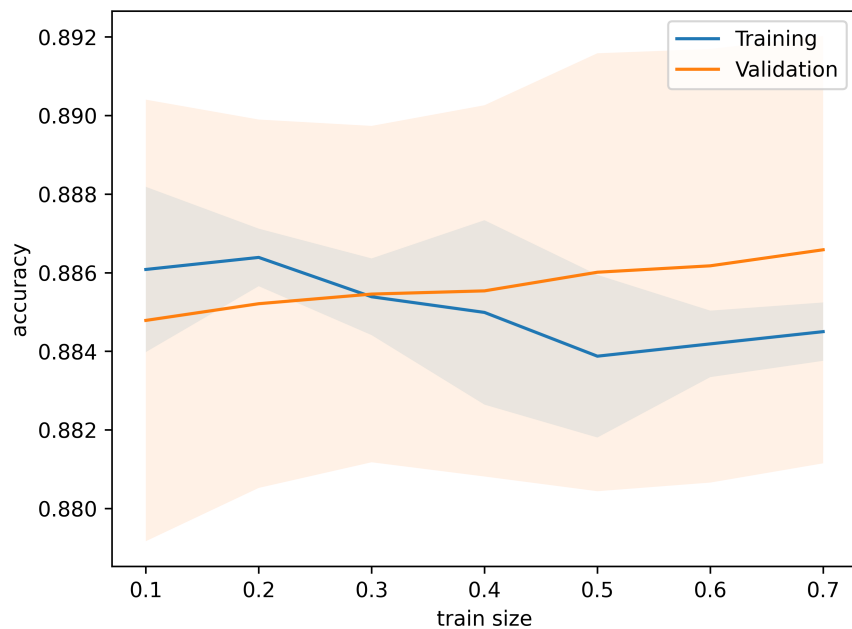


**Fig. S13.** Learning curves for a Multilayer Perceptron classifier applied to the dataset of toric varieties of Picard rank two and dimension at least six. The plot shows the means of the training and validation accuracies for five different random train–test splits. The shaded regions correspond to the  $1\sigma$  interval, where  $\sigma$  denotes the standard deviation.

ML models		
SVM with linear kernel	Random Forest Classifier	MLP neural network
87.69%	88.61%	89.03%

**Table S3.** Accuracies for a linear SVM, RFC, and MLP applied to the dataset of toric varieties of Picard rank two and dimension at least six.

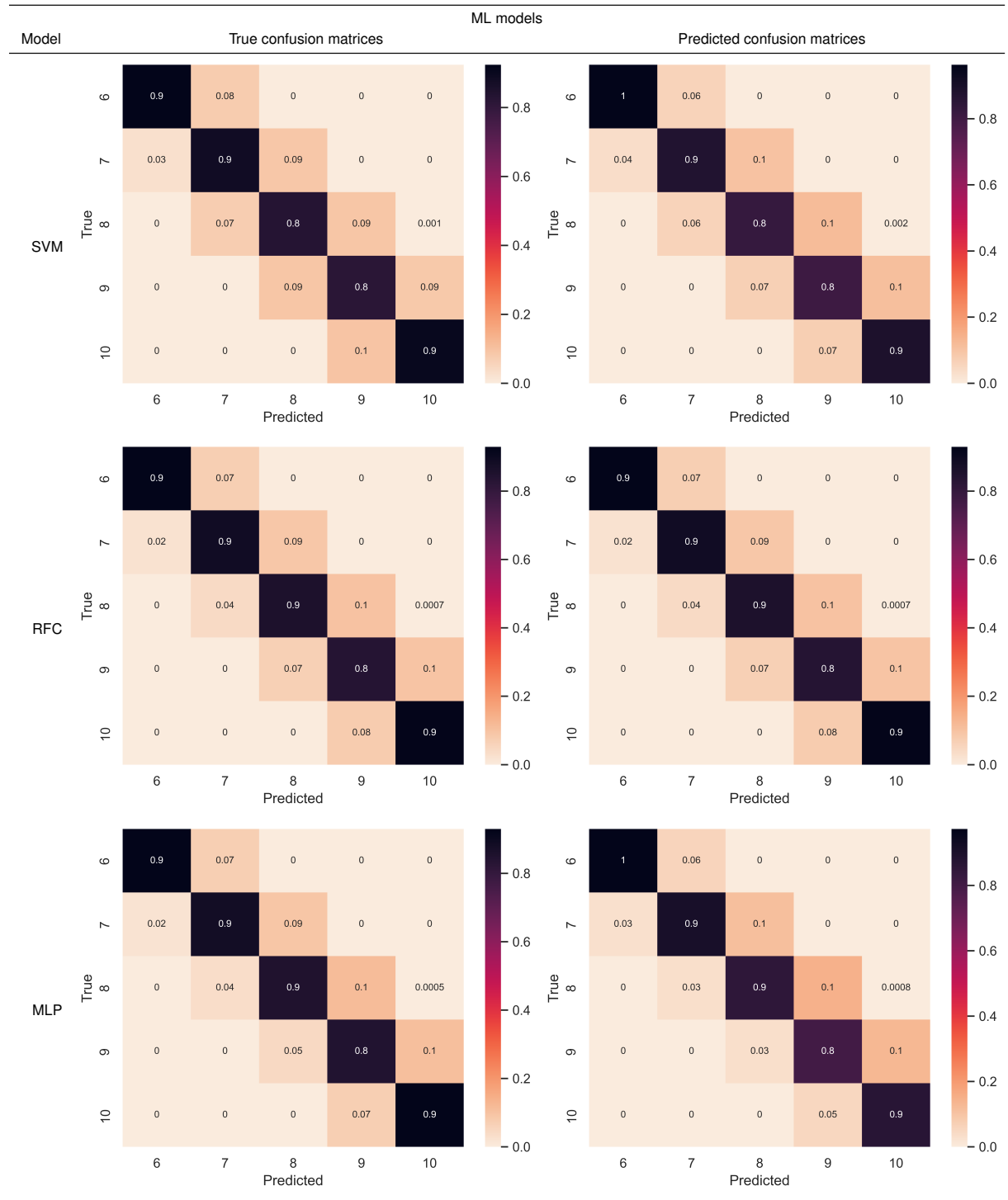


**Table S4.** Confusion matrices for a linear SVM, RFC, and MLP applied to the dataset of toric varieties of Picard rank two and dimension at least six.

## References

1. Dolgachev I (1982) Weighted projective varieties in *Group actions and vector fields (Vancouver, B.C., 1981)*, Lecture Notes in Math. (Springer, Berlin) Vol. 956, pp. 34–71.
2. Iano-Fletcher AR (2000) Working with weighted complete intersections in *Explicit birational geometry of 3-folds*, London Math. Soc. Lecture Note Ser. (Cambridge Univ. Press, Cambridge) Vol. 281, pp. 101–173.
3. Coates T, Corti A, Galkin S, Kasprzyk AM (2016) Quantum periods for 3-dimensional Fano manifolds. *Geom. Topol.* 20(1):103–256.
4. Fulton W (1993) *Introduction to toric varieties*, Annals of Mathematics Studies. (Princeton University Press, Princeton, NJ) Vol. 131, pp. xii+157. The William H. Roever Lectures in Geometry.
5. Cox DA, Little JB, Schenck HK (2011) *Toric varieties*, Graduate Studies in Mathematics. (American Mathematical Society, Providence, RI) Vol. 124, pp. xxiv+841.
6. Brown G, Corti A, Zucconi F (2004) Birational geometry of 3-fold Mori fibre spaces in *The Fano Conference*. (Univ. Torino, Turin), pp. 235–275.
7. Kasprzyk AM (2006) Toric Fano three-folds with terminal singularities. *Tohoku Math. J. (2)* 58(1):101–121.
8. Pedregosa F, et al. (2011) Scikit-learn: Machine learning in Python. *Journal of Machine Learning Research* 12:2825–2830.
9. Coates T, Kasprzyk AM, Veneziale S (2022) Supporting code (<https://bitbucket.org/fanosearch/mldim>).
10. Kingma DP, Ba J (2014) Adam: A method for stochastic optimization. [arXiv:1412.6980 \[cs.LG\]](https://arxiv.org/abs/1412.6980).
11. Agarap AF (2018) Deep learning using rectified linear units (ReLU). [arXiv:1803.08375 \[cs.NE\]](https://arxiv.org/abs/1803.08375).
12. Gnedenko BV, Ushakov IA (2018) *Theory of probability*. (Routledge).
13. Kasprzyk AM (2013) Classifying terminal weighted projective space. [arXiv:1304.3029 \[math.AG\]](https://arxiv.org/abs/1304.3029).